Journal of Materials Chemistry A

ROYAL SOCIETY OF CHEMISTRY

REVIEW

View Article Online
View Journal | View Issue

Cite this: J. Mater. Chem. A, 2026, 14, 8452

A review on strategies toward high-mass-loading aqueous zinc-ion batteries

Yan Ran, Huaping Zhao and Yong Lei *

High-mass-loading electrodes are indispensable for the practical implementation of aqueous zinc-ion batteries (AZIBs); however, their performance is often constrained by sluggish ion/electron transport, structural instability, and the incomplete utilization of active materials. This review summarizes recent advances in addressing these challenges through advances in both material innovation and electrode engineering. Cathode developments are discussed, including manganese-based compounds, vanadium-based materials, transition metal dichalcogenides, and other emerging high-capacity systems. Key structural strategies are further highlighted, encompassing the optimization of conductive additives, modifications of binders and current collectors, fabrication of freestanding electrodes, and the employment of three-dimensional (3D) printing to construct precise and scalable architectures. The integration of these approaches enables the development of high-mass-loading AZIB cathodes with enhanced energy density, rate capability, and cycling durability. This review provides an overview of practical design principles and future directions for advancing high-performance AZIBs.

Received 6th October 2025
Accepted 27th December 2025

DOI: 10.1039/d5ta08145a

rsc.li/materials-a

1. Introduction

The excessive reliance on traditional fossil fuels has led to severe environmental degradation, energy crises, and global climate change, posing a significant threat to the sustainable development of both the planet and human society.[1–3] Consequently, the shift toward renewable energy, especially sources that are clean and naturally abundant, has become an unavoidable global trend and a critical requirement for long-term sustainability. However, the intermittent and unstable nature of renewable energy sources such as solar and wind power necessitates the development of large-scale and reliable energy storage systems to ensure a stable energy supply and efficient energy utilization. Since the 1990s, lithium-ion batteries (LIBs) have dominated the energy storage market and have been widely adopted in many aspects of daily life, including portable electronics and electric vehicles.[4,5] Despite their widespread application, LIBs face several challenges that

Fachgebiet Angewandte Nanophysik, Institut für Physik & IMN MacroNano, Technische Universität Ilmenau, 98693 Ilmenau, Germany. E-mail: yong.lei@tu-ilmenau.de

Yan Ran

Yan Ran received her Master's degree in Materials Physics and Chemistry from Yunnan University in 2022. She is currently a PhD candidate under the supervision of Prof. Yong Lei at the Technical University of Ilmenau in Germany. Her research interests focus on the design and synthesis of nanostructured materials and their applications in aqueous zinc ion batteries and electrocatalysis.

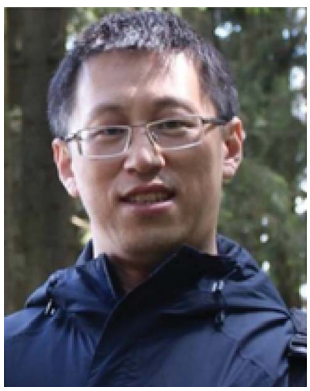

Huaping Zhao

Huaping Zhao obtained his PhD in materials science from the State Key Laboratory of Crystal Materials at Shandong University in 2007. Following 2 years of postdoctoral research at the Institute of Chemistry (Chinese Academy of Sciences, 2007–2009), he was employed as a scientist by the University of Muenster from 2009 to 2011. Since 2012, he has been a senior scientist (permanent) in Prof. Yong Lei's group at the Technical University of Ilmenau, Germany. His current research focus is the design and fabrication of functional nanostructures for energy storage and conversion.

limit their broader deployment, such as safety concerns associated with flammable organic electrolytes, insufficient energy density for grid-scale use, and the rising cost and uneven distribution of lithium resources.[2,5–7] These issues have stimulated intensive research efforts toward the development of alternative energy storage technologies that are safer, more cost-effective, and more sustainable.

Among various candidates, aqueous zinc-ion batteries (AZIBs) have emerged as one of the most promising next-generation energy storage devices due to their unique advantages (Fig. 1). These include low redox potential (−0.76 V *vs.* SHE), high theoretical capacity (820 mAh g^{-1}) and volumetric capacity (5855 mAh cm^{-3}), cost-effectiveness, intrinsic safety, and environmental friendliness.[6,8–10] The use of mild aqueous electrolytes eliminates the risk of flammability, making AZIBs particularly suitable for grid-scale and stationary storage applications.[11] Despite these advantages, the development of low-cost and high-efficiency cathode materials for reversible Zn^{2+} storage remains a major challenge. A variety of cathode materials have been investigated, including manganese-based compounds, vanadium-based oxides, Prussian blue analogs (PBAs), organic materials, and other metal-based frameworks.[1,11–13] However, it is important to note that the electrochemical performance of most AZIBs is often evaluated under idealized laboratory conditions, particularly under low mass loadings (<2 mg cm^{-2}), to achieve high specific capacities and excellent rate performance.[14–16] These conditions, while beneficial for fundamental research, fail to represent the true behavior of AZIBs under practical, commercial-level requirements. As the mass loading of active materials increases toward practical values (>10 mg cm^{-2}), a series of critical issues arises.[17,18] Thicker electrodes hinder ionic diffusion and electron transport, leading to poor electrochemical utilization and significant capacity loss. Additionally, the reduced interfacial contact between the electrode and the electrolyte further deteriorates performance, resulting in decreased energy density, poor cycling stability, and lower overall efficiency.[19] Simply increasing the mass of cathode materials without carefully designing the electrode structure often leads to diminished returns and inefficient energy storage.[16,20] Therefore, achieving high-mass loading cathodes without sacrificing performance is a crucial step toward the practical application of AZIBs. This requires a careful balance between increasing active material content and maintaining rapid charge transport and efficient ion diffusion throughout the electrode.[21–23]

To address these challenges, various strategies have been proposed and demonstrated. These include (i) the design of advanced electrode architectures to shorten ion/electron pathways; (ii) the use of conductive additives and flexible binders to enhance mechanical integrity and electrical conductivity; (iii) electrolyte optimization to improve ionic conductivity and electrode wetting; and (iv) the development of scalable electrode fabrication techniques that maintain structural integrity and electrochemical performance under thick configurations. Furthermore, the choice and engineering of cathode materials play a pivotal role in enabling high-mass loading operations. For instance, vanadium-based oxides with layered or tunnel structures can be modified *via* interlayer expansion, cation pre-intercalation, or hybridization with carbonaceous components to promote ion accessibility and structural stability.[25,26] Similarly, manganese-based materials and PBAs offer low cost and structural diversity but require modification to suppress dissolution and improve conductivity at large thicknesses.[27,28] Although numerous reviews have summarized the material design and electrochemical mechanisms of AZIBs, the majority have primarily emphasized low-mass-loading conditions and laboratory-scale performance metrics. In contrast, the practical deployment of AZIBs necessitates overcoming challenges that arise under high areal mass loading, including sluggish ion transport, incomplete utilization of active materials, and mechanical instability. To date, only a limited number of reviews have systematically addressed strategies specifically tailored to high-loading conditions, which are crucial for bridging the gap between academic research and commercial implementation.

This review provides a comprehensive overview of recent progress and future perspectives on strategies for achieving high-mass loading in AZIBs (Fig. 2). It begins with a discussion of the fundamental challenges associated with increased electrode mass loading, such as limited ion and electron transport, structural instability, and so on. Advances in cathode material development are then summarized, encompassing manganese-based compounds and various vanadium-based materials such as vanadium pentoxide, metal vanadates, and other vanadium derivatives, as well as transition metal dichalcogenides and other emerging high-capacity systems. In addition to material innovation, key structural engineering strategies are examined, including the conductive additive regulations, binder modifications, current collector regulation, free-standing structures, and three-dimensional (3D) printing. This review provides a timely and focused summary of recent advancements in materials and

Yong Lei

Yong Lei is a Professor and Head of the Department of Applied Nano-Physics at the Technical University of Ilmenau, Germany. He began working in Germany in 2003 as an Alexander von Humboldt Fellow at the Karlsruhe Institute of Technology. From 2006, he worked at the University of Muenster as a group leader and a Junior Professor. In 2011, he joined the Technical University of Ilmenau as a Professor. His research focuses include template nanostructuring, energy conversion and storage devices, and optoelectronic applications of nanostructures. He has received a few prestigious EU and German research grants including two European Research Council Grants. He is an Advisory Board Member or Associate Editor of Advanced Energy Materials, Energy & Environmental Materials, Small, InfoMat, Carbon Energy, and Science China Materials.

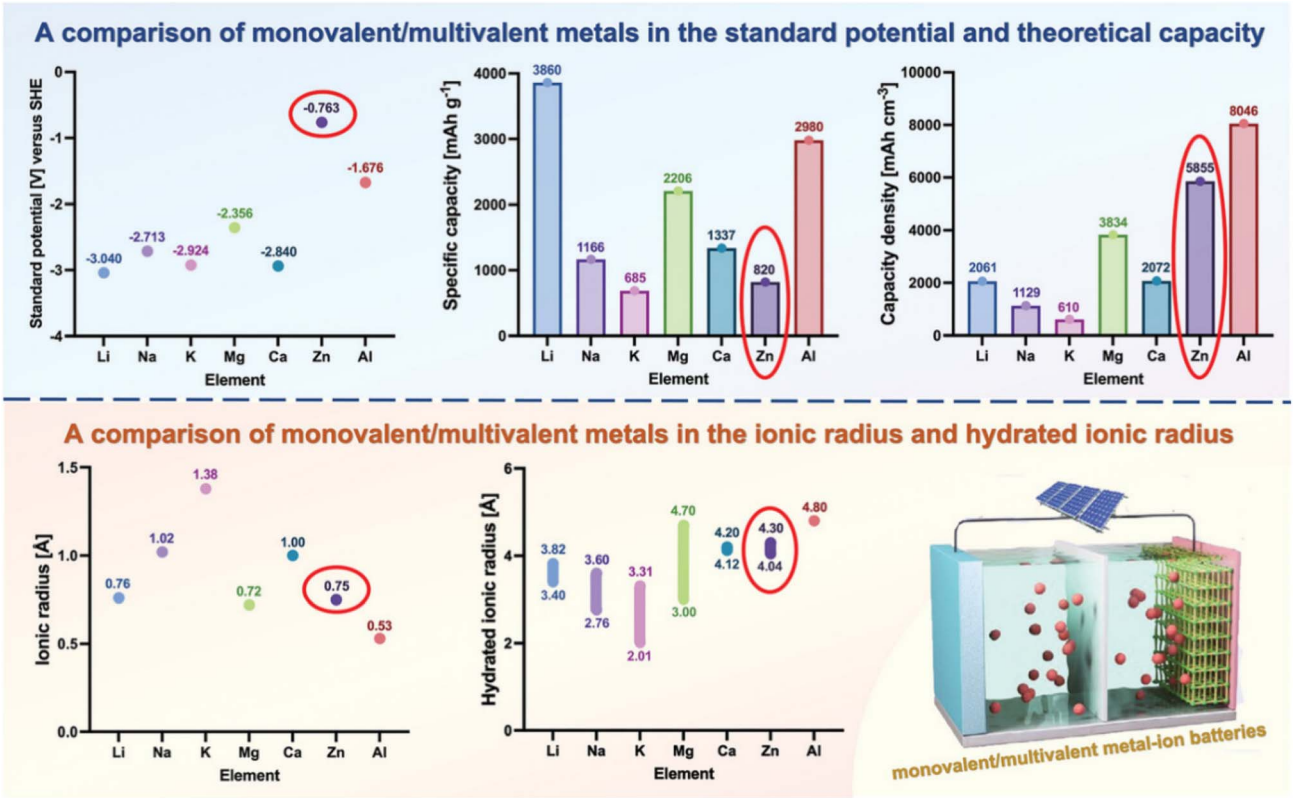

Fig. 1 The comparisons of monovalent/multivalent metals with respect to the standard potential and theoretical capacity (top), ionic radius, and hydrated ionic radius (bottom). Reproduced from ref. 24 with permission from Wiley-VCH, copyright 2023.

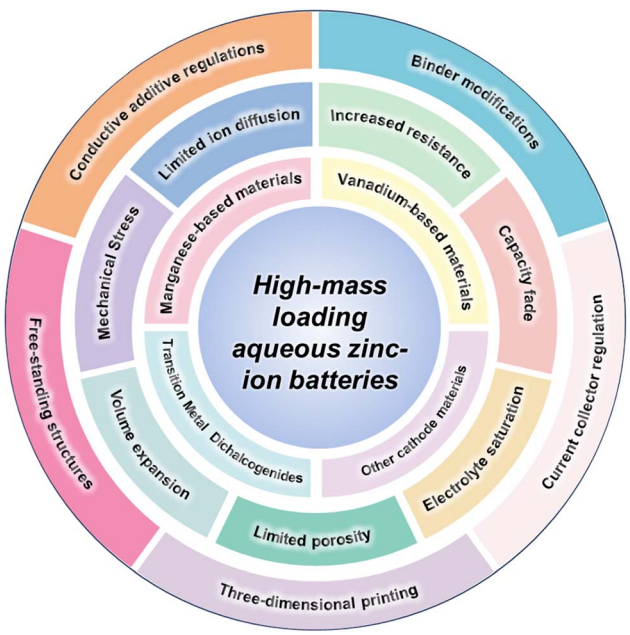

Fig. 2 Schematic illustration of material and structural strategies for high-mass-loading aqueous zinc-ion batteries.

structural design strategies specifically aimed at achieving high-mass loading in AZIBs, offering insights into practical optimization routes and future development directions.

2. Challenges of high-loading cathodes for aqueous zinc-ion batteries

Maximizing the areal capacity in the cathode material is the most direct and effective way to increase the energy density of AZIBs in practical applications, which can be attributed to the reduction in the weight fraction of inactive components such as binders and current collectors. Therefore, rationally designing the thickness of the cathode material is an effective strategy to increase the load capacity. In addition, increasing the thickness can reduce the proportion of inactive components in the battery, including electrolytes, separators, and current collectors, thereby increasing the energy density of AZIBs. However, preparing high-mass loading electrode materials simply by isoproportional methods of low-loading structures will bring new challenges. Therefore, how to increase the loading capacity and capacity of the cathode material without affecting the electrochemical performance faces some new difficulties, as follows:

(1) Limited ion diffusion: in high-mass-loading electrodes, sluggish ion diffusion becomes a critical bottleneck for electrochemical performance. As the electrode thickness increases, Zn^{2+} ions must traverse a longer diffusion pathway to reach the interior active sites. This not only prolongs ion transport time but also leads to uneven charge distribution

across the electrode depth, where the surface layers participate actively in the reaction while the inner regions remain underutilized. Such inhomogeneous ion accessibility can cause local concentration gradients, severe polarization, and reduced utilization of the active material. Moreover, the inherently sluggish kinetics of Zn^{2+} insertion/extraction, compared with monovalent cations such as Li^{+}, exacerbate this issue under thick-electrode conditions. As a consequence, the electrochemical system often exhibits slower charge–discharge rates, diminished rate capability, and compromised cycling stability.

(2) Increased resistance: as the electrode mass loading increases, the overall internal resistance of the cathode tends to increase due to both electronic and ionic transport limitations. In thick electrodes, electrons must travel longer distances through the active material and binder matrix, which inevitably introduces higher ohmic losses. Simultaneously, densely stacked particles can hinder electrolyte penetration and ion migration, leading to elevated interfacial resistance and sluggish charge-transfer processes. These resistive effects become more pronounced at high current densities, where rapid transport of both electrons and ions is essential to sustain reversible redox reactions. The consequence is often manifested as increased polarization, reduced energy efficiency, and incomplete utilization of the active material.

(3) Capacity fade: thick electrodes are often more prone to capacity degradation during long-term cycling compared with their low-loading counterparts. The larger volume of active material amplifies internal stresses generated by repeated ion insertion and extraction, which can induce particle cracking, delamination, or collapse of the electrode architecture. In addition, sluggish ion and electron transport in thick structures can cause uneven reaction kinetics across the electrode depth, leading to preferential utilization of surface regions while interior regions remain underused. This inhomogeneous activity accelerates localized degradation and exacerbates overall capacity fading. Furthermore, the extended diffusion pathways and high tortuosity of thick electrodes may aggravate side reactions, electrolyte depletion, and accumulation of inactive by-products, further reducing cycle stability.

(4) Mechanical stress: high-mass-loading electrodes are also vulnerable to mechanical stresses arising from repeated ion insertion and extraction. During cycling, the expansion and contraction of active materials induce significant strain within the thick electrode, which is further amplified by the limited structural flexibility of densely packed layers. Over time, this stress can cause microcracks, particle pulverization, and loss of interparticle contact, thereby increasing internal resistance and reducing electronic/ionic connectivity. Such mechanical degradation not only lowers the reversible capacity but also accelerates electrode delamination from the current collector, ultimately shortening cycle life.

(5) Volume expansion: electrodes with high-mass-loading are particularly susceptible to volume changes during repeated charge–discharge cycles. Significant expansion and contraction of the active material can induce mechanical instability, promoting microcracking, delamination from the current collector, and loss of interparticle contact. These effects not only compromise electronic and ionic connectivity but also exacerbate polarization and accelerate capacity fading. The issue becomes more severe in thick electrodes due to the cumulative strain distributed throughout the bulk, which can lead to heterogeneous reactions and localized degradation.

(6) Electrolyte saturation: in high-mass-loading electrodes, ensuring uniform electrolyte distribution throughout the bulk can be challenging. Thick electrodes often have densely packed structures and high tortuosity, which can hinder electrolyte infiltration and ion transport. As a result, certain regions may experience electrolyte depletion or even local dry-out, leading to uneven ionic conductivity and reaction rates across the electrode. This non-uniformity can exacerbate polarization, reduce active material utilization, and accelerate capacity fading. In severe cases, poor electrolyte saturation can also compromise battery safety by increasing local overpotentials and promoting side reactions.

(7) Limited porosity: as electrode mass loading increases, the overall porosity of the electrode often decreases due to the densely packed active material and binder. Reduced porosity limits the pathways available for electrolyte penetration and ion transport, which can result in slower reaction kinetics and uneven utilization of active sites. Consequently, portions of the electrode may remain electrochemically inactive, reducing the effective capacity and lowering both energy and power densities. Additionally, limited porosity can exacerbate issues such as localized concentration gradients, polarization, and poor thermal management within the electrode.

Although it is easy to say that increasing cathode mass loading increases the areal capacity and, consequently, the theoretical energy density of Zn-ion cells, interconnected transport, mechanical, and electrochemical constraints limit the strategy's practical application in full-cell architectures. Thicker electrodes tend to increase tortuosity and extend the effective diffusion pathways for Zn ions and co-transporting species, causing uneven charge distribution, steep concentration gradients during cycling, and greater ohmic and concentration overpotentials. At the same time, electron percolation becomes increasingly difficult. Without a robust and homogeneous conductive network, regions farther from the current collector may experience electronic starvation and poor utilization of active materials. Mechanically, thicker electrodes also tend to concentrate volumetric strain and stress, promoting particle fracture, binder-particle detachment, and interfacial delamination, all of which deteriorate long-term cycling stability and increase cell impedance. All these shortcomings may reduce the electrochemical performance of high-load AZIBs. Therefore, how to design high-load operating electrodes close to the theoretical specific capacity remains a major obstacle. Characterization, understanding and improving ion transport kinetics of high-loading cathode materials remain at the research frontier of AZIBs, playing a crucial role in achieving high energy density of batteries as well as practical commercial applications. Beyond the cathode itself, mass and capacity balancing at the cell level imposes stringent design constraints. Achieving a high areal cathode capacity requires either a sufficiently large Zn reservoir or highly efficient Zn utilization to

prevent premature anode depletion. However, excessive Zn loading reduces the overall gravimetric and volumetric energy densities, thereby diminishing the practical energy metrics of the cell. In addition, the intensified local Zn^{2+} fluxes at high cathode loadings aggravate nonuniform Zn plating and stripping, which promotes dendritic growth, parasitic side reactions (such as hydrogen evolution and local pH fluctuations), and accelerated anode corrosion. The degradations occurring at the anode side alter cell polarization and the electrolyte environment, which in turn impact the cathode behavior and give rise to a coupled degradation pathway that should be carefully considered in the design of high-loading cells. Moreover, the electrolyte also plays a decisive role in achieving high energy density in AZIBs. Under high-loading conditions, the electrolyte must sustain fast ion transport while maintaining interfacial stability with both electrodes. Insufficient ion accessibility or excessive polarization within the thick cathode can alter local Zn^{2+} concentrations and disturb the solvation structure, which may intensify parasitic reactions and by-product accumulation. Rational electrolyte design through optimizing salt concentration, introducing functional additives, or adopting hybrid aqueous-organic systems can help regulate Zn^{2+} solvation and suppress side reactions. Meanwhile, the electrolyte composition should provide adequate wettability and mechanical compatibility with thick electrodes to minimize transport heterogeneity and ensure long-term reversibility. Therefore, electrolyte optimization should be regarded as an integral part of the high-loading strategy to achieve both high energy density and durable cycling stability. Nevertheless, in this review, we focus primarily on the cathode side. While electrolyte optimization and anode behavior under high-loading conditions are important for ensuring stable operation, the main strategies discussed here concern the design, structure, and fabrication of cathode materials. For the cathode, recent efforts have been devoted to addressing the challenges of high-loading designs through various approaches, such as the rational design of cathode materials, the construction of self-supporting architectures without binders, conductive additives, or current collectors, and the application of advanced fabrication techniques like 3D printing. These strategies have shown promising potential for achieving high-mass-loading cathodes in AZIBs and form the main focus of this review.

3. Aqueous zinc-ion batteries with high loading cathodes

The cathode is an important part of the battery. In recent years, most of the research on AZIBs has focused on the research and development of cathode materials. In practical electrode design, especially high load electrodes, this design approach provides several advantages for the performance and practical applications of these batteries. such as higher power output and high energy density, making them suitable for applications that require rapid energy discharge. Not only that, but high-load electrodes often exhibit improved cycling stability because they can distribute the stress and strain associated with charge and discharge cycles more effectively, which can extend the battery's cycle life. Here, we summarize the research in recent years on the design of high-mass loading cathode materials for AZIBs (Table 1) and systematically analyze the principles and effects of these materials on the construction of AZIBs. In this review, high-mass-loading cathode materials are categorized into four main classes for detailed discussion: manganese-based materials, vanadium-based materials, transition metal dichalcogenides, and other types.

3.1 Manganese-based materials

Manganese is one of the most abundant transition metals in the Earth's crust, and its compounds have been extensively employed in areas such as catalysis, desulfurization, and electrochemical energy storage owing to their rich valence chemistry (Mn^{2+}, Mn^{3+}, Mn^{4+}, and Mn^{7+}).[62,63] The intrinsic advantages of Mn-based compounds, including structural diversity, the ability to accommodate a wide range of cations such as Zn^{2+}, low toxicity, environmental benignity, and low cost, make them particularly attractive for AZIB applications.[64] In electrochemical systems, Mn-based cathodes can operate through multiple charge storage pathways, including Zn^{2+} intercalation/deintercalation, conversion-type reactions, and dissolution–redeposition processes, which together contribute to their promising rate capability and energy density.[65] Within this family, manganese dioxide (MnO_2) has emerged as the most representative cathode material, owing to its polymorphic nature that provides diverse ion diffusion channels and structural tunability.[66] Moreover, MnO_2 can be synthesized through facile and cost-effective routes, and its electrochemical properties can be further optimized *via* defect regulation, heteroatom substitution, or integration with conductive hosts. These merits render MnO_2 and its derivatives central to the development of high-mass-loading cathodes for practical AZIBs, and thus a focal point of current research. We will discuss high-mass loading manganese-based cathodes for AZIBs in the following sections.

3.1.1 MnO_2. MnO_2 is regarded as one of the most representative cathode materials for AZIBs, owing to its abundance, low cost, and environmental friendliness.[65] A distinctive advantage of MnO_2 lies in its multiple crystallographic polymorphs (α-, β-, γ-, δ-, λ-, and ε-types), which differ in framework topology such as tunnel, layered, or spinel configurations.[2,27] These structural variations provide diverse Zn^{2+} storage pathways and lead to markedly different electrochemical responses. As summarized in Table 2, the intrinsic structural features of MnO_2 polymorphs not only dictate Zn^{2+} storage mechanisms but also influence their applicability in high-mass-loading cathodes. Efficient ion transport and robust structural frameworks are indispensable for thick electrodes to perform reliably. For instance, tunnel-type MnO_2 generally offers high theoretical capacity but faces kinetic limitations under large electrode thickness, while layered δ-MnO_2 with its open interlayer galleries, is particularly advantageous for sustaining Zn^{2+} diffusion at high loading.[67] Spinel λ-MnO_2, featuring a 3D transport network, also holds promise for balancing capacity

Table 1 The electrochemical performance of high-mass loading cathode materials for AZIBs reported in recent years

Materials	Mass loading	Electrolyte	Specific capacity	Cycle numbers	Ref.
MnO_2	28.4 mg cm^{-2}	1 M $ZnSO_4$ and 0.1 M $MnSO_4$	288.8 mAh g^{-1} at 0.1 A g^{-1}	—	29
B-MnO_2	30 mg cm^{-2}	2 M $ZnSO_4$ and 0.2 M $MnSO_4$	311.9 mAh g^{-1} at 0.2 A g^{-1}	2000 cycles at 2 A g^{-1}	30
H-d-MnO_2	10 mg cm^{-2}	2 M $ZnSO_4$ and 0.1 M $MnSO_4$	221.4 mAh g^{-1} at 0.2 C	250 cycles at 1 C	31
Mxene@MnO_2	8 mg cm^{-2}	2 M $ZnSO_4$ and 0.1 M $MnSO_4$	301.2 mAh g^{-1} at 0.1 A g^{-1}	2000 cycles at 0.5 A g^{-1}	32
CEI-A@MnO_2	23.6 mg cm^{-2}	2 M $ZnSO_4$ and 0.2 M $MnSO_4$	232 mAh g^{-1} at 50 mA g^{-1}	5000 cycles at 3 A g^{-1}	33
CEI-A@$ZnMn_2O_4$	25.2 mg cm^{-2}	2 M $ZnSO_4$ and 0.2 M $MnSO_4$	138 mAh g^{-1} at 0.1 A g^{-1}	5000 cycles at 2 A g^{-1}	33
MnOOH	15 mg cm^{-2}	2 M $ZnSO_4$ and 0.1 M $MnSO_4$	178 mAh g^{-1} at 0.1 A g^{-1}	500 cycles at 0.5 A g^{-1}	34
$K_{0.37}MnO_2 \cdot 0.54H_2O$/C	4 mg cm^{-2}	2 M $ZnSO_4$ and 0.2 M $MnSO_4$	302.4 mAh g^{-1} at 0.1 A g^{-1}	1000 cycles at 2 A g^{-1}	35
VO_2	15 mg cm^{-2}	3 M $Zn(CF_3SO_3)_2$	332 mAh g^{-1} at 0.62 C	2000 cycles at 6.2 C	36
V^{5+}-VO_2@PPy	20 mg cm^{-2}	3 M $Zn(CF_3SO_3)_2$	345.5 mAh g^{-1} at 10 A g^{-1}	1000 cycles at 2 A g^{-1}	15
VO_2(B)@CFS	4.5 mg cm^{-2}	1 M $ZnSO_4$	396.7 mAh g^{-1} at 0.1 A g^{-1}	1000 cycles at 2 A g^{-1}	37
VO_x	6 mg cm^{-2}	6 M $ZnCl_2$	402 mAh g^{-1} at 0.26 A g^{-1}	10 000 cycles at 7.8 A g^{-1}	38
Graphene-analogous $V_2O_5 \cdot nH_2O$	10.2 mg cm^{-2}	2 M $Zn(CF_3SO_3)_2$	714 mAh g^{-1} at 0.1 A g^{-1}	1000 cycles at 2 A g^{-1}	39
P-$V_2O_5 \cdot nH_2O$ @P	5 mg cm^{-2}	3 M $Zn(CF_3SO_3)_2$	345 mAh g^{-1} at 0.1 A g^{-1}	2000 cycles at 2 A g^{-1}	40
$V_5O_{12} \cdot 6H_2O$-LGO	26.5 mg cm^{-2}	3 M $Zn(ClO_4)_2$	467 mAh g^{-1} at 0.1 A g^{-1}	10 000 cycles at 10 A g^{-1}	41
$V_3O_7 \cdot H_2O$	12 mg cm^{-2}	3 M $Zn(CF_3SO_3)_2$	321 mAh g^{-1} at 0.1 A g^{-1}	800 cycles at 2 A g^{-1}	42
$V_6O_{13} \cdot H_2O$	10 mg cm^{-2}	2 M $Zn(CF_3SO_3)_2$	217 mAh g^{-1} at 1 A g^{-1}	500 cycles at 1 A g^{-1}	43
VO-C2PC	9.79 mg cm^{-2}	2 M $Zn(OTf)_2$	102 mAh g^{-1} at 5 A g^{-1}	5000 cycles at 5 A g^{-1}	44
CaV_4O_9/CNT	50 mg cm^{-2}	3 M $Zn(CF_3SO_3)_2$	352 mAh g^{-1} at 0.1 A g^{-1}	3000 cycles at 10 A g^{-1}	45
PEG-$Ba_{0.38}V_2O_5 \cdot nH_2O$	4 mg cm^{-2}	2 M $ZnSO_4$	289 mAh g^{-1} at 0.5 A g^{-1}	4000 cycles at 6 A g^{-1}	46
rGO/δ-$Na_xV_2O_5 \cdot nH_2O$	5 mg cm^{-2}	2 M $ZnSO_4$	374.9 mAh g^{-1} at 0.1 A g^{-1}	4000 cycles at 2 A g^{-1}	47
NVO ⊂ CNTs	12 mg cm^{-2}	3 M $Zn(CF_3SO_3)_2$	460.2 mAh g^{-1} at 0.5 A g^{-1}	2500 cycles at 10 A g^{-1}	48
PTEMPO-4/MWCNTs	8 mg cm^{-2}	2 M $Zn(OTf)_2$	70 mAh g^{-1} at 5 C	300 cycles at 5 C	49
VN/N-rGO	13 mg cm^{-2}	3 M $Zn(CF_3SO_3)_2$	390 mAh g^{-1} at 0.05 A g^{-1}	30 cycles at 0.05 A g^{-1}	19
$K_{0.486}V_2O_5$	10 mg cm^{-2}	15 M $ZnCl_2$	419.4 mAh g^{-1} at 0.05 A g^{-1}	1400 cycles at 3 A g^{-1}	50
$Cu_{0.18}V_2O_5 \cdot 0.72H_2O$	7 mg cm^{-2}	3 M $Zn(CF_3SO_3)_2$	223.4 mAh g^{-1} at 1 A g^{-1}	2000 cycles at 1 A g^{-1}	51
$Mg_{0.26}V_2O_5 \cdot 0.73H_2O$	5 mg cm^{-2}	3 M $Zn(CF_3SO_3)_2$	2.1 mAh cm^{-2} at 0.05 A g^{-1}	2000 cycles at 5 A g^{-1}	52
Li@MnVO	10 mg cm^{-2}	3 M $Zn(CF_3SO_3)_2$	342 mAh g^{-1} at 0.1 A g^{-1}	5000 cycles at 10 A g^{-1}	53
$H_{11}Al_2V_6O_{23.2}$@graphene	15.7 mg cm^{-2}	2 M $ZnSO_4$	305.4 mAh g^{-1} at 1 A g^{-1}	400 cycles at 2 A g^{-1}	54
3DP-FeVO/rHGO	24.4 mg cm^{-2}	2.5 M $Zn(CF_3SO_3)_2$	344.8 mAh g^{-1} at 0.1 A g^{-1}	650 cycles at 2 A g^{-1}	55
FA-$VOPO_4$	10 mg cm^{-2}	2 M $Zn(CF_3SO_3)_2$	173 mAh g^{-1} at 1 A g^{-1}	2000 cycles at 2 A g^{-1}	56
VS_2@SS	~11 mg cm^{-2}	1 M $ZnSO_4$	187 mAh g^{-1} at 0.1 A g^{-1}	2000 cycles at 2 A g^{-1}	57
Rose D-VS_2	10 mg cm^{-2}	2 M $Zn(OTf)_2$	285 mAh g^{-1} at 0.1 A g^{-1}	200 cycles at 0.5 A g^{-1}	58
MoS_2	~11.5 mg cm^{-2}	3 M $ZnSO_4$	181.8 mAh g^{-1} at 0.1 A g^{-1}	2100 cycles at 10 A g^{-1}	22
$MnCO_3$	7.2 mg cm^{-2}	3 M $ZnSO_4$ and 0.1 M $MnSO_4$	280 mAh g^{-1} at 50 mA g^{-1}	2000 cycles at 1 A g^{-1}	59
α-MoO_3@CFC	15 mg cm^{-2}	2 M $ZnSO_4$	200.8 mAh g^{-1} at 0.2 A g^{-1}	500 cycles at 1 A g^{-1}	60
C@multi-layer polymer	10.2 mg cm^{-2}	2 M $ZnSO_4$	302 mAh g^{-1} at 0.1 A g^{-1}	5000 cycles at 5 A g^{-1}	61

and rate capability in practical devices.[68] Guided by these structural insights, recent studies have focused on strategies such as phase engineering, compositional tuning, and hybridization with conductive matrices to fully exploit the potential of MnO_2 in high-mass-loading AZIB cathodes.

For example, Deng *et al.*[30] proposed a molecular engineering strategy to construct boron-modified MnO_2 (B-MnO_2) with improved intrinsic electronic and ionic conductivity *via* a facile one-step hydrothermal process (Fig. 3a). The resulting Zn//B-MnO_2 batteries delivered a high specific capacity of 299.2 mAh g^{-1} at 0.1 A g^{-1} even under a high-mass-loading of 10.0 mg cm^{-2} (Fig. 3b). Remarkably, when the mass loading was further increased to 25 and 30 mg cm^{-2}, the capacities were still maintained at 197.2 and 176.5 mAh g^{-1}, respectively (Fig. 3c). This performance enhancement is mainly attributed to the incorporation of boron atoms with low electronegativity, which effectively narrows the band gap of MnO_2 to improve its intrinsic electronic/ionic conductivity and simultaneously alleviates the strong electrostatic interactions between Zn^{2+} ions and the cathode framework, thereby accelerating reaction kinetics. Wu *et al.*[69] employed a simple ethanol-mediated hydrothermal approach to construct rod-like β-MnO_2 nanostructures with tailored oxygen vacancies. By precisely adjusting the amount of ethanol introduced during synthesis, the concentration of oxygen vacancies could be effectively optimized, leading to enhanced electronic conductivity and increased exposure of active sites. When β-MnO_{2-x}-5 was used as the cathode material, the cell achieved an areal capacity of 5 mAh cm^{-2} (corresponding to 357 mAh g^{-1} and 469.8 Wh kg^{-1}) at a high-mass-loading of 14 mg cm^{-2}. In addition, rational nanostructure engineering of MnO_2 has proven to be an effective strategy for improving cathode performance. Shang *et al.*[16] reported the fabrication of defect-rich MnO_2 (d-MnO_2) nanosheets through an interface-assisted synthesis, followed by phosphidation, phase conversion, and freeze-drying processes, thereby constructing a freestanding high-mass-loading electrode (Hd-MnO_2). Benefiting from the optimized chemical composition and nanoscale architecture, the d-MnO_2 nanosheets exhibited accelerated electrochemical kinetics, enhanced conductivity arising from abundant defects, and additional Zn

Table 2 Structural characteristics of typical MnO_2 polymorphs and their relevance to high-mass-loading cathodes in AZIBs

Polymorph	Structure type	Ion transport characteristics	Features in AZIBs	Implications for high-mass-loading electrodes
α-MnO_2	2 × 2 tunnel	Large tunnels allow insertion of hydrated Zn^{2+} ions	High theoretical capacity, but structural instability during deep cycling	Capable of storing large amounts of Zn^{2+}, yet stability challenges are amplified under high loading
β-MnO_2	1 × 1 tunnel	Very narrow tunnels restrict Zn^{2+} diffusion	Excellent structural stability, but low capacity	Limited utilization in thick electrodes due to sluggish kinetics
γ-MnO_2	Mixed tunnels (1 × 1 and 1 × 2)	Multiple ion transport channels	Balanced capacity and cycling stability	Suitable for moderate loadings; ion transport may still be insufficient for very thick electrodes
δ-MnO_2	Layered	Wide interlayer spacing, expandable by water/ions	High reversible capacity; fast Zn^{2+} kinetics	Particularly advantageous for high-mass-loading designs due to facile ion diffusion across thick layers
λ-MnO_2	Spinel	3D interconnected tunnels	Good rate performance and decent stability	Promising for high-power thick electrodes, but synthesis is more complex
ε-MnO_2	Disordered tunnel/layered	High surface activity; short diffusion paths	Enhanced reactivity but less structural order	Effective in composite electrodes at high loadings, though prone to side reactions

storage sites. Moreover, the binder-free porous Hd-MnO_2 electrode, free of electrochemically inert current collectors, facilitated electrolyte penetration and enabled high energy density. As a result, the Hd-MnO_2 cathode delivered an impressive energy density of up to 265 Wh kg^{-1} and an initial areal capacity of ~2.73 mAh cm^{-2} at a mass loading of 10 mg cm^{-2}. This freestanding and defect-engineered high-mass-loading electrode design offers a promising route for advancing Mn-based cathodes toward practical energy-related applications.

In summary, high-mass-loading MnO_2 cathodes possess several intrinsic advantages, including natural abundance, low cost, multiple crystal polymorphs, and flexible structural tunability, all of which contribute to their potential for delivering high specific capacity and energy density. Nevertheless, when applied at practical mass loadings, MnO_2-based cathodes still encounter a series of critical challenges. The repeated insertion and extraction of Zn^{2+} and H^+ ions often induce severe lattice strain and phase transformations, leading to mechanical degradation and loss of active sites. Meanwhile, the intrinsically low electronic conductivity and sluggish ion diffusion become more pronounced in thick electrodes, resulting in pronounced polarization and limited utilization of the active material. Furthermore, dissolution and subsequent redeposition of Mn species during cycling not only cause irreversible capacity decay but also form uneven by-products that block ion pathways and deteriorate electrode integrity. To address these issues, future research should focus on rational phase and defect engineering to stabilize the crystal framework and enhance intrinsic conductivity, as well as the design of hierarchical and porous architectures that facilitate electrolyte penetration and shorten ion/electron transport paths. Introducing conductive networks or flexible binders can also improve mechanical robustness and charge transport in thick electrodes. Combining these strategies will be essential to balance capacity, rate performance, and long-term stability, ultimately promoting the practical deployment of MnO_2-based cathodes in AZIBs.

3.1.2 Manganates. Manganates represent one of the earliest and most extensively studied cathode systems for AZIBs, prized for their structural diversity, natural abundance, and environmental compatibility. Their frameworks, constructed from corner- or edge-sharing [MnO_6] octahedra, form layered or tunnel-type architectures that provide open channels for Zn^{2+} and H^+ insertion/extraction and enable redox activity through the Mn^{4+}/Mn^{3+} couple.[28,70] In typical systems such as $ZnMnO_4$, Mn can also undergo higher–valence transitions ($Mn^{6+}/Mn^{7+} \leftrightarrow Mn^{4+}/Mn^{3+}$), affording high theoretical capacities often exceeding 300 mAh g^{-1} and elevated operating voltages.[6,71,72] However, when moving toward practical implementation with high-mass-loading electrodes, the inherent structural and kinetic limitations of manganates become more prominent. At high areal loadings, the dense stacking of the active material significantly impedes ion and electron transport, leading to increased polarization and incomplete redox utilization of the inner regions. Simultaneously, the repeated insertion/extraction of multivalent ions under large capacity swings intensifies lattice distortion, triggering phase transformation and promoting Mn dissolution *via* the disproportionation of Mn^{3+} ($2Mn^{3+} \rightarrow Mn^{2+} + Mn^{4+}$).[27,28] The dissolved Mn^{2+} not only depletes the active material but also participates in parasitic redeposition reactions, further damaging electrode integrity and cycle stability. Moreover, poor interfacial contact between the thick manganate layer and current collector aggravates charge-transfer resistance, limiting rate performance. To overcome these challenges, current research emphasizes structure

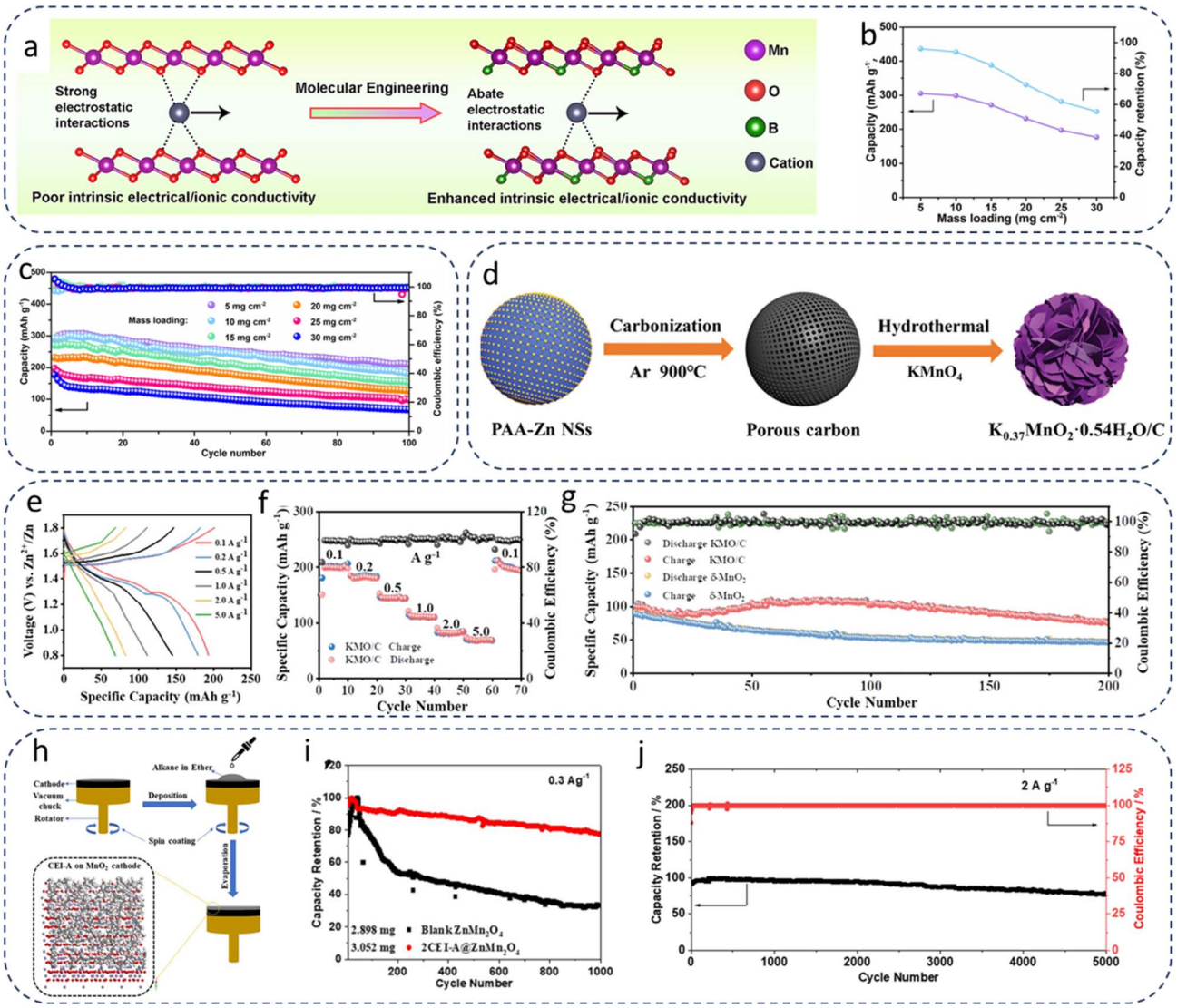

Fig. 3 (a) Molecular tailoring schematic illustration of B-MnO_2. (b) Specific capacity and capacity retention, and (c) cycling performance at 0.1 A g^{-1} of B-MnO_2 cathodes with different mass loadings (1, 5, 10, 15, 20, 25, and 30 mg cm^{-2}). Reproduced from ref. 30 with permission from Elsevier, copyright 2023. (d) Synthesis process of KMO/C. (e) GCD curves of the KMO/C cell at different current densities. (f) Rate performance of the KMO/C cell. (g) Long-term cycling performance of δ-MnO_2 and KMO/C cells. Reproduced from ref. 35 with permission from Wiley-VCH, copyright 2023. (h) Schematic illustration of an artificial CEI composed of alkane-based paraffin on the cathode surface. (i) Cycling performance at 0.3 A g^{-1}. (j) Cycling performance of the 2CEI-A@ZMO assembled large battery with a high-mass-loading of 25.2 mg cm^{-1} at 2 A g^{-1}. Reproduced from ref. 33 with permission from American Chemical Society, copyright 2022.

stabilization and electrode architecture engineering. Strategies such as pre-insertion of stabilizing cations (*e.g.*, Zn^{2+}, Ba^{2+}, and Cu^{2+}) can suppress Jahn–Teller distortion and mitigate Mn dissolution, while conductive carbon networks and hierarchical porous structures improve electron pathways and electrolyte accessibility in thick electrodes.[62] Surface coatings or gradient compositions further buffer structural stress and enhance interfacial durability. By integrating these approaches, high-mass-loading manganate cathodes can achieve a balanced combination of high capacity, structural robustness, and long-term cycling stability, advancing their potential for practical AZIB applications.

Potassium manganate is one of the few manganates that have been reported for high-mass-loading cathodes. As illustrated in Fig. 3d, Jia *et al.*[35] designed a composite electrode ($K_{0.37}MnO_2 \cdot 0.54H_2O$/C, denoted as KMO/C) *via* a hydrothermal method using porous carbon nanospheres as the substrate. Benefiting from its unique hybrid structure, the KMO/C//Zn battery exhibited excellent electrochemical performance at room temperature. Specifically, at a current density of 2 A g^{-1}, the electrode delivered a capacity of 127.3 mAh g^{-1} after 1000 cycles, corresponding to an average capacity decay of only 0.0019% per cycle. Furthermore, additional tests under high-mass-loading (4 mg) confirmed that KMO/C maintained well-defined GCD curves and demonstrated satisfactory rate capability (Fig. 3e and f) and cycling stability (Fig. 3g). More importantly, the simple two-electrode configuration composed of KMO/C and Zn was able to spontaneously undergo redox

reactions in a mildly acidic electrolyte, thereby achieving self-charging behavior without any external power supply. This work highlights the promise of KMO/C electrodes for practical applications, particularly under harsh conditions and high-mass-loading configurations, offering valuable insights into the development of advanced manganate-based cathodes. In addition to potassium manganate, zinc manganate has also been investigated as another representative manganate for high-mass-loading applications, showing complementary structural advantages and electrochemical properties. In contrast, zinc manganate inherently incorporates Zn^{2+} into the crystal lattice, which not only stabilizes the structure but also mitigates Mn dissolution, a notorious degradation pathway in Mn-based electrodes. Liu *et al.*[33] advanced this concept by introducing a paraffin-based artificial cathode–electrolyte interface (CEI) to further suppress Mn^{2+} dissolution and graphite corrosion (Fig. 3h), enabling $ZnMn_2O_4$ cathodes to maintain outstanding electrochemical stability under extreme mass loadings. The CEI-A modified $ZnMn_2O_4$ cathode exhibited a capacity retention of 81% after 1000 cycles at a current density of 0.3 A g^{-1}, indicating that the CEI-A modification significantly enhanced the capacity retention of the ZMO cathode (Fig. 3i). Remarkably, Zn//$ZnMn_2O_4$ full cells with paraffin CEI retained 78% of their capacity after 5000 cycles at a very high cathode mass loading of 25.2 mg cm^{-2} (Fig. 3j), outperforming most Mn-based cathodes reported to date. Such results underscore that $ZnMn_2O_4$, with intrinsic lattice stabilization from Zn^{2+} and extrinsic interfacial engineering, holds unique promise for bridging the gap between laboratory-scale performance and practical deployment of AZIBs.

Therefore, for manganates, future research should therefore focus on rational structural engineering and interface modification to suppress Mn dissolution and mitigate structural degradation. In addition, synergistic strategies such as cation pre-intercalation, surface functionalization, hybridization with conductive frameworks, and electrolyte optimization are expected to further enhance their electrochemical stability. Combining these approaches with advanced *in situ* characterization and theoretical modeling will provide deeper insights into the charge storage mechanisms of manganates, ultimately accelerating their translation from laboratory studies to practical, large-scale AZIB applications.

3.2 Vanadium-based materials

Compared with manganese-based systems, vanadium-based materials offer additional advantages for constructing high-mass-loading cathodes in AZIBs.[73] The multiple valence states of vanadium (V^{2+} to V^{5+}) and its flexible coordination environments enable rich redox chemistry and diverse Zn^{2+} storage mechanisms.[74,75] In particular, layered vanadium oxides and hydrated vanadates provide large interlayer spacing and structural tunability, which are beneficial for accommodating Zn^{2+} ions, facilitating fast transport, and mitigating mechanical stress under thick-electrode conditions.[8,73] Moreover, the high theoretical capacities of vanadium compounds make them especially attractive for achieving high areal energy density when the electrode mass loading is increased.[10] In this section, we summarize recent progress on vanadium-based cathodes for high-mass-loading AZIBs, with emphasis on three representative categories: vanadium pentoxide, metal vanadates, and other vanadium-based derivatives.

3.2.1 Vanadium pentoxide. Vanadium pentoxide (V_2O_5) is one of the most representative vanadium-based cathode materials for aqueous zinc-ion batteries, owing to its natural abundance, low cost, and high theoretical capacity (~589 mAh g^{-1}).[76] Its layered crystal structure, composed of VO_5 square pyramids, can accommodate guest cations and water molecules between layers, offering large diffusion channels for Zn^{2+} insertion/extraction and partially buffering lattice strain during cycling. The multiple redox states of vanadium ($V^{5+}/V^{4+}/V^{3+}$) endow V_2O_5 with rich electrochemical activity and high capacity potential, which are particularly advantageous for high-mass-loading electrodes seeking to achieve elevated areal energy densities.[77] However, under high-mass-loading, the intrinsic limitations of V_2O_5 become significantly magnified. The low intrinsic electronic conductivity and sluggish Zn^{2+} diffusion kinetics hinder charge transfer through the thick electrode, resulting in severe polarization and incomplete activation of the interior active regions. Meanwhile, repeated Zn^{2+} intercalation/extraction induces pronounced lattice distortion and irreversible phase evolution, leading to mechanical degradation, volume pulverization, and capacity fading during long-term cycling. The poor mechanical cohesion within the thick V_2O_5 layer and weak interfacial contact with the current collector further exacerbate these issues, collectively impeding rate performance and electrochemical stability. To address these challenges, extensive efforts have been devoted to interlayer engineering, structural hydration, doping, and conductive hybridization, aiming to enhance transport properties and stabilize the V_2O_5 framework under high-loading conditions.

Linghu *et al.*[44] proposed a strategy that integrates structural engineering with electrolyte modulation, in which hierarchical porous V_2O_5 nanosheet arrays (VO-C2) were *in situ* constructed on carbon cloth through electrodeposition followed by calcination, while propylene carbonate (PC) was introduced as an electrolyte additive (Fig. 4a). This design not only improved electronic conductivity and electrolyte wettability but also effectively suppressed the dissolution of V_2O_5. During cycling, V_2O_5 gradually transformed into a more stable zinc pyrovanadate (ZVO) phase (Fig. 4b), whose lower bandgap and enlarged interlayer spacing helped to buffer volume fluctuations and enhance ion transport stability. Across a wide range of mass loadings (1.00–9.79 mg cm^{-2}), the electrode demonstrated excellent structural integrity and electrochemical performance; even at a high loading of 9.79 mg cm^{-2}, and it still delivered a capacity of 311 mAh g^{-1} and maintained favorable capacity retention after 5000 cycles (Fig. 4c and d). This dual optimization of the structure and electrolyte provides valuable insights into achieving long-term durability in thick electrodes. Complementarily, Wu *et al.*[78] approached the problem from the perspective of structural and compositional regulation. Through a solution-based reaction, they converted tunnel-type α-V_2O_5 into ultrathin layered nanosheets and further

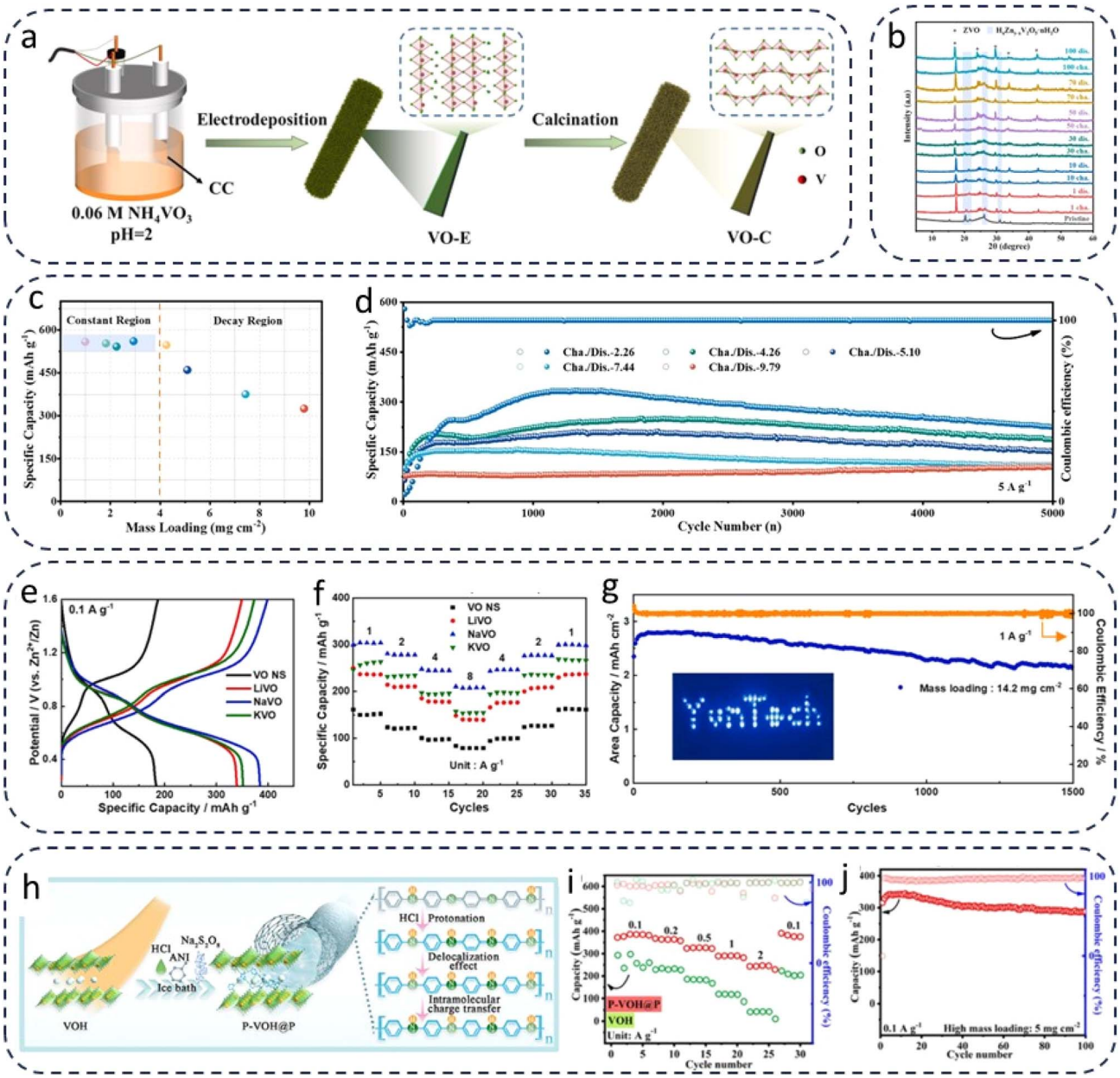

Fig. 4 (a) Schematic of the fabrication procedure. (b) *Ex situ* XRD patterns of VO-C2PC before/after various cycles. (c) Relationship between specific capacity and mass loading. (d) Long-term cycling stability. Reproduced from ref. 44 with permission from Elsevier, copyright 2024. (e) GCD curves at 0.1 A g^{-1} and (f) rate performance of VO NS, LiVO, NaVO, and KVO. (g) Cycle performance of NaVO/MWCNTs cathodes. Reproduced from ref. 78 with permission from Elsevier, copyright 2024. (h) Schematic diagram of the synthesis of the core–shell P-VOH@P heterostructure; morphology of the core–shell P-VOH@P heterostructure. (i) Rate performance of the Zn//P-VOH@P cell and Zn//VOH cell. (j) Cycling performance of the Zn//P-VOH@P cell with high-mass-loading at 0.1 A g^{-1}. Reproduced from ref. 40 with permission from Wiley-VCH, copyright 2022.

introduced alkali-metal-ion (particularly Na^+) pre-intercalation to form $Na_xV_8O_{20}\cdot nH_2O$ (NaVO). The resulting material exhibited wider diffusion channels, higher surface area, and a narrower bandgap, which significantly improved both ionic and electronic transport kinetics. Electrochemical testing revealed that NaVO delivered a high specific capacity of 383 mAh g^{-1} at 0.1 A g^{-1} (Fig. 4e) and maintained 207 mAh g^{-1} even at 8 A g^{-1} (Fig. 4f), demonstrating excellent rate capability. More importantly, when integrated with multi-walled carbon nanotubes (MWCNTs) to construct a freestanding high-mass-loading electrode, the system achieved an areal capacity of 3.2 mAh cm^{-2} at a mass loading of ~14.2 mg cm^{-2} and sustained long-term cycling stability, with a cumulative capacity output of 3.7 Ah cm^{-2} after 1500 cycles (Fig. 4g). Building on this, Sun *et al.*[40] proposed a "three-in-one" strategy to optimize the structure and performance of $V_2O_5\cdot nH_2O$ nanobelts (P-VOH@P) by simultaneously intercalating and encapsulating them with protonated polyaniline (PANI) (Fig. 4h). In this design, the intercalated

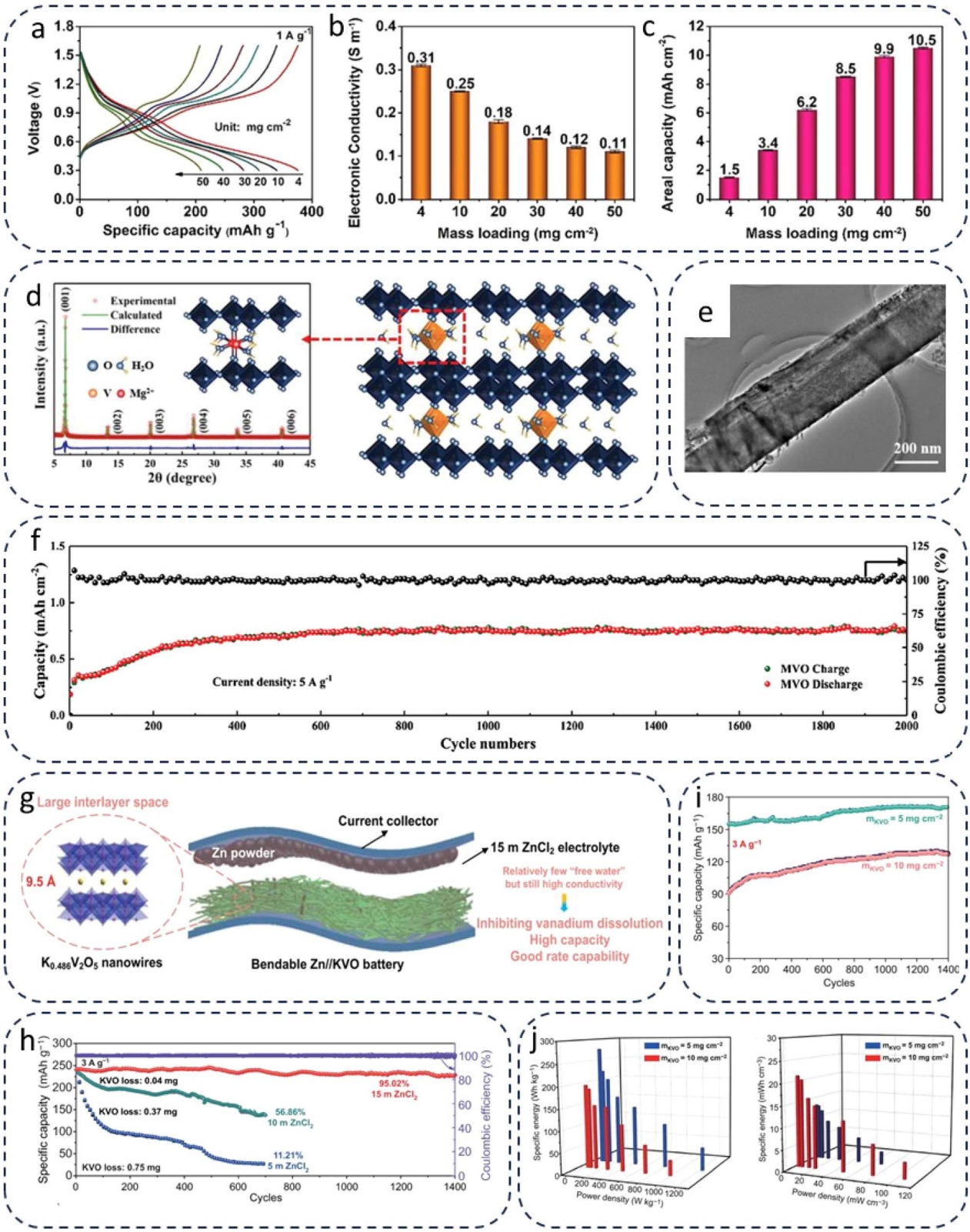

Fig. 5 (a) Charge/discharge curves of CaVO/CNTs electrodes with different mass loadings. (b) The corresponding electronic conductivity. (c)The corresponding areal capacity. Reproduced from ref. 45 with permission from Elsevier, copyright 2022. (d) Rietveld refinement result of the Mg^{2+}-stabilized $V_2O_5{\cdot}0.73H_2O$ XRD pattern and the corresponding crystal structure. (e) TEM image. (f) Cycling performance at 5 A g^{-1}. Reproduced from ref. 52 with permission from Wiley-VCH, copyright 2020. (g) Schematic illustration of the bendable Zn//$K_{0.486}V_2O_5$ cell with controlled electrolyte concentration. (h) Cycle stability comparison in 5, 10, and 15 m $ZnCl_2$ electrolytes at 3 A g^{-1}. (i) Cycling performance. (j) Energy densities and power densities of the cell based on $K_{0.486}V_2O_5$ mass and the volume of the device. Reproduced from ref. 50 with permission from Springer, copyright 2020.

PANI pillars expanded the interlayer spacing and weakened the electrostatic interactions between [VO] units and Zn^{2+}, thereby accelerating Zn^{2+} diffusion kinetics. Meanwhile, the PANI shell stabilized the heterostructure and mitigated structural degradation during cycling. In addition, protonated PANI enhanced the overall conductivity and contributed extra capacity through reversible intrachain electronic migration. Benefiting from these synergetic effects, the Zn//P-VOH@P cell delivered 387 mAh g^{-1} at a low mass loading of 2 mg cm^{-2} (Fig. 4i) and retained 345 mAh g^{-1} at a higher loading of 5 mg cm^{-2} (Fig. 4j), while also exhibiting low capacity decay and good rate capability. This study demonstrates the potential of conductive polymer intercalation and encapsulation to simultaneously achieve high capacity, cycling stability, and rate performance under thick-electrode conditions, offering a promising pathway for the structural engineering of high-mass-loading vanadium-based cathodes.

All in all, V_2O_5 shows great promise as a high-mass-loading cathode owing to its high theoretical capacity and layered framework, yet its intrinsic conductivity and structural stability issues under thick-electrode conditions remain major challenges. Recent advances, including hierarchical porous design with electrolyte modulation, structural reconstruction with alkali-ion pre-intercalation, and conductive polymer intercalation/encapsulation, have demonstrated effective ways to enhance ion transport, conductivity, and durability at practical mass loadings. These studies highlight the importance of integrated structural and compositional engineering in enabling stable, high-performance V_2O_5 cathodes, and also provide useful insights for extending similar strategies to other vanadium-based systems.

3.2.2 Metal vanadates. Metal vanadates represent another important branch of vanadium-based cathodes for aqueous zinc-ion batteries. Benefiting from the variable valence states of vanadium and the flexible V–O polyhedral framework, metal vanadates can accommodate diverse cation species through intercalation.[73] Such cation incorporation not only expands the interlayer spacing of vanadium oxides, thereby facilitating Zn^{2+} diffusion, but also exerts a "pillar effect" that reinforces the layered framework and suppresses lattice breathing, ultimately enhancing structural stability and cycling durability.[11,70] To date, a wide range of cations, including alkali metals (Li^+, Na^+, and K^+), alkaline earth metals (Ca^{2+} and Mg^{2+}), transition metals (Cu^{2+} and Ag^+), and even nonmetallic species (NH_4^+), have been introduced to construct metal vanadates with improved electrochemical properties.[24] Particularly under high-mass-loading conditions, the stabilized frameworks and enlarged interlayer galleries of metal vanadates are advantageous for sustaining efficient ion transport and maintaining electrode integrity. Moreover, hydrated metal vanadates, with intercalated water molecules, offer additional structural flexibility and ion-conduction pathways, further broadening their potential as robust cathodes for practical thick-electrode configurations.

Du *et al.*[45] constructed a flexible freestanding electrode by integrating CaV_4O_9 microflowers with carbon nanotubes (CaVO/CNTs). During the initial charge process, Ca^{2+} ions were irreversibly extracted, leading to the transformation of CaV_4O_9 into amorphous $V_2O_5 \cdot nH_2O$. Compared with its crystalline counterpart, this amorphous phase provided more active sites, while the carbon nanotubes enhanced electronic conductivity, enabling the electrode to deliver a high specific capacity of 410 mAh g^{-1} (Fig. 5a). Remarkably, even at an ultrahigh-mass-loading of ~50 mg cm^{-2}, the electrode maintained an areal capacity of 10.5 mAh cm^{-2} (Fig. 5b and c). Building on this, Wang *et al.*[52] reported Mg^{2+}-stabilized $V_2O_5 \cdot 0.73H_2O$ nanobelts (Fig. 5d and e). The synergistic pillar effect of Mg^{2+} and structural water effectively mitigated lattice contraction and facilitated Zn^{2+} diffusion kinetics, allowing the electrode to achieve an areal capacity of 2.12 mAh cm^{-2} at a mass loading of 5 mg cm^{-2}, while maintaining 98% capacity retention after 2500 cycles at a high rate of 10 A g^{-1} (Fig. 5f). In addition, Jiang *et al.*[46] introduced a Ba^{2+} intercalation strategy, which further demonstrated the unique advantages of alkaline-earth-metal incorporation in stabilizing layered frameworks. Benefiting from the large ionic radius of Ba^{2+}, $Ba_{0.38}V_2O_5 \cdot nH_2O$ exhibited expanded interlayer spacing and reinforced structural stability, thereby delivering fast Zn^{2+} transport and long-term cycling durability under high-mass-loading conditions. Collectively, these studies highlight that alkaline-earth-metal intercalation not only plays a crucial role in optimizing microstructural stability and ion transport dynamics, but also offers a practical pathway to achieve the balance between high capacity and long cycle life in thick-electrode configurations.

In addition to alkaline-earth vanadates, alkali-metal vanadates have also demonstrated distinctive advantages under high-mass-loading conditions. Taking $K_{0.486}V_2O_5$ as an example, this material features a large interlayer spacing (~0.95 nm), which provides rapid diffusion pathways for the reversible insertion/extraction of Zn^{2+} and endows it with a high theoretical capacity. However, the dissolution of vanadium-based materials in conventional dilute electrolytes severely compromises their cycling stability. To address this issue, Li *et al.*[50] proposed an electrolyte engineering strategy (Fig. 5g). They demonstrated that in a moderately concentrated $ZnCl_2$ electrolyte (15 m), $K_{0.486}V_2O_5$ maintained ~95.02% capacity retention after 1400 cycles, representing a significant improvement in stability (Fig. 5h). Furthermore, the authors developed, for the first time, a sodium carboxymethyl cellulose (CMC)-based $ZnCl_2$ gel electrolyte with high ionic conductivity (10.08 mS cm^{-1}) and successfully assembled a flexible quasi-solid-state battery. Even at high-mass-loadings of 5 and 10 mg cm^{-2}, the device exhibited outstanding cycling stability (Fig. 5i) along with impressive energy and power densities (Fig. 5j). This work not only confirmed the promise of potassium vanadates as high-mass-loading cathodes but also highlighted the feasibility of using moderately concentrated electrolytes to mitigate dissolution issues, offering a new perspective for the practical application of vanadium-based electrodes. Tang *et al.*[47] further advanced this field by fabricating a flexible freestanding rGO/d-$Na_xV_2O_5 \cdot nH_2O$ nanocomposite paper electrode *via* a facile vacuum filtration method. The electrode achieved an active material loading of 5 mg cm^{-2}, substantially higher than that of most reported flexible binder-free electrodes (typically <2 mg

cm^{-2}). Benefiting from the homogeneous distribution and synergistic interaction of active nanobelts, carbon nanotubes, and cellulose fibers, the electrode exhibited both excellent mechanical flexibility and high electrical conductivity. Electrochemically, it delivered an areal capacity of 1.87 mAh cm^{-2} (corresponding to 374.9 mAh g^{-1}) at a loading of 5 mg cm^{-2}, which surpasses that of most flexible AZIB electrodes reported to date. In addition, the electrode demonstrated good rate capability and long-term cycling durability, retaining 92% of its capacity after 4000 cycles. This study provides a feasible pathway for constructing flexible, binder-free vanadate electrodes that simultaneously achieve high-mass-loading and robust electrochemical performance.

In summary, both alkaline-earth vanadates such as CaV_4O_9/CNT, $Mg_{0.26}V_2O_5 \cdot 0.73H_2O$, and $Ba_{0.38}V_2O_5 \cdot nH_2O$, and alkali-metal vanadates including $K_{0.486}V_2O_5$ and $Na_xV_2O_5 \cdot nH_2O$, have achieved significant breakthroughs in capacity retention and cycling stability under high-mass-loading conditions through ion pre-intercalation and structural engineering strategies. Alkaline-earth systems mainly rely on the "pillar effect" to stabilize the layered framework and enhance Zn^{2+} diffusion, whereas alkali-metal systems exhibit advantages in interlayer regulation and the construction of flexible electrodes. Collectively, these studies demonstrate that metal-ion intercalation combined with multidimensional structural optimization represents a key pathway for advancing vanadate cathodes toward practical applications in thick electrodes and flexible energy-storage devices.

3.2.3 Other vanadium-based materials. Apart from the extensively studied V_2O_5 and metal vanadates, a few other vanadium-based compounds have also been explored as cathodes for high-mass-loading AZIBs. Although their reports are relatively limited, these materials exhibit distinctive structural features and electrochemical behaviors that provide valuable insights into the design of thick electrodes.

VO_2 has attracted considerable attention owing to its reversible phase transition characteristics and high theoretical capacity. Ma *et al.*[36] constructed a VO_2-based nanoarray electrode to address the ion diffusion limitations typically encountered in thick electrodes (Fig. 6a). By growing vertically aligned VO_2 nanosheet arrays directly on a conductive substrate, the design significantly enhanced the electrode–electrolyte interfacial contact and shortened Zn^{2+} diffusion pathways (Fig. 6b and c). Even under a high-mass-loading exceeding 10 mg cm^{-2}, the electrode maintained a high specific capacity and favorable rate performance, while also exhibiting stable capacity retention during long-term cycling (Fig. 5d). This study demonstrates that array engineering is an effective strategy to mitigate ion transport bottlenecks in thick electrodes, thereby offering new insights into the development of VO_2 cathodes for high-mass-loading applications. Wei *et al.*[41] employed a graphene-composite strategy that not only enhanced the electronic conductivity of the electrode but also introduced a distinctive "pseudo-Zn–air" mechanism through oxygen-containing functional groups on the graphene surface. In this system, the intercalation/deintercalation of Zn^{2+} ions operated synergistically with oxygen reduction/oxidation reactions, leading to a dual energy-storage mechanism. As a result, the electrode delivered an impressive areal capacity of 10.6 mAh cm^{-2} under an ultrahigh-mass-loading of 26.5 mg cm^{-2} (Fig. 6e). More importantly, it retained 84.7% of its capacity even after 10 000 cycles, far surpassing most reported thick-electrode systems (Fig. 6f). These findings clearly demonstrate that interfacial chemistry regulation combined with multi-reaction mechanisms can markedly enhance both capacity and cycling stability under high-mass-loading conditions. Chen *et al.*[18] successfully fabricated high-loading $V_3O_7 \cdot H_2O$ nanowire array electrodes through a combination of solution-phase synthesis and arrayed design (Fig. 6g). Benefiting from the presence of crystallization water in the layered structure, the material can effectively accommodate volume changes and enhance ion diffusion kinetics during Zn^{2+} insertion/extraction. Electrochemical measurements indicate that even under a high electrode loading of 12 mg cm^{-2}, the electrode maintains a specific capacity of approximately 200 mAh g^{-1} (Fig. 6h). Further analysis reveals a two-stage energy storage mechanism, where the reversible Zn^{2+} intercalation and the synergistic effect of crystallization water jointly preserve the structural integrity of the electrode and enable long-term cycling stability (Fig. 6i). This work highlights that rational control of crystallization water combined with arrayed structural design can significantly improve the practical performance of vanadate electrodes under high-loading conditions. In addition, the $H_{11}Al_2V_6O_{23} \cdot 2H_2O$ material proposed by Zhang *et al.*[54] further demonstrates the potential of ion doping and conductive composites in thick electrodes. As shown in Fig. 6j, the introduction of Al^{3+} into the (001) crystal plane expands the interlayer spacing up to 13.36 Å, providing wide diffusion channels for Zn^{2+} and significantly alleviating kinetic limitations in thick electrodes. Meanwhile, the incorporation of graphene effectively enhances electronic conductivity and suppresses the dissolution of active species in the electrolyte. Even under an ultrahigh electrode loading of 15.7 mg cm^{-2}, the electrode retains a capacity of 131.7 mAh g^{-1} after 400 cycles, demonstrating the feasibility of simultaneously achieving high capacity and long-term stability under high-loading conditions (Fig. 6k).

Although research on other types of vanadium-based materials remains relatively limited, significant progress has been achieved under high-loading conditions through multiple strategies, including arrayed design, interfacial chemistry regulation, and the synergistic effect of crystallization water, as well as ion doping and conductive composites. These studies indicate that rational structural engineering and composite design can not only substantially enhance ion transport and structural stability in thick electrodes, but also strike a balance between energy density and cycle life, providing new insights and directions for the practical application of vanadium-based materials in high-loading AZIBs.

3.3 Transition metal dichalcogenides

In the preceding sections, we reviewed the advances in manganese- and vanadium-based materials for high-

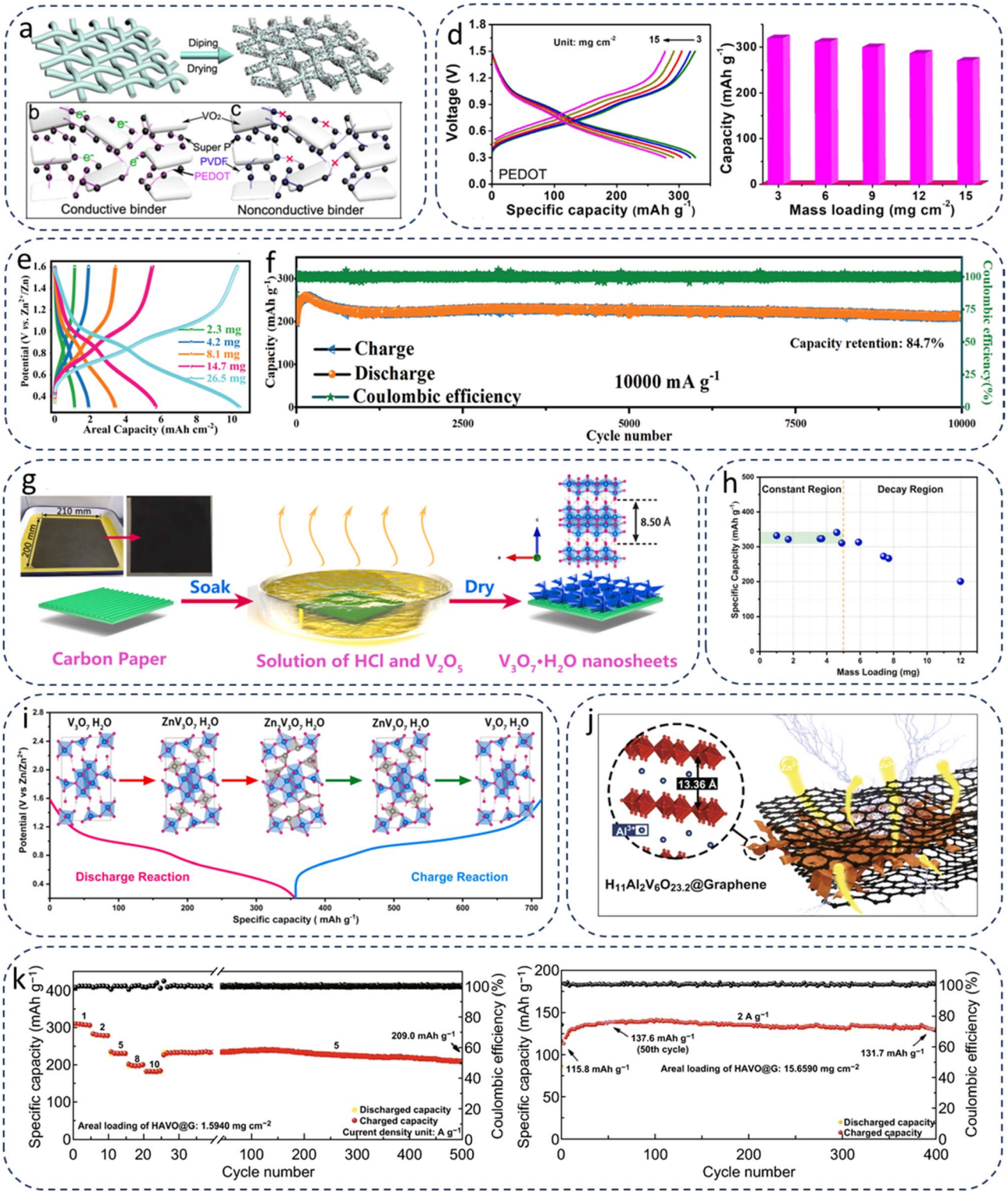

Fig. 6 (a) Schematic illustrating the assembling strategy of VO_2 cathodes on a 3D current collector. Schematic diagrams of the VO_2 cathodes with a (b) conductive binder and (c) nonconductive binder. (d) The galvanostatic discharge/charge curves and corresponding capacities of different mass loading cathodes assembled with a 3D current collector and conductive binder. Reproduced from ref. 36 with permission from Elsevier, copyright 2020. (e) Galvanostatic charge–discharge curves of electrodes under different mass loadings at a current density of 0.1 A g^{-1} in the voltage window of 0.3–1.6 V (*vs.* Zn/Zn^{2+}). (f) Cycling performances at a current density of 10 A g^{-1} of VO-LGO. Reproduced from ref. 41 with permission from Wiley-VCH, copyright 2019. (g) Schematic of the one-step synthesis process for the binder-free VOHA electrode. (h) The specific capacity of VOHAs at various mass loadings. All of the results were collected at a specific current of 0.1 A g^{-1}. (i) Schematic of the stepwise uptake/extraction process of Zn^{2+} at different discharge/charge depths. Reproduced from ref. 18 with permission from Elsevier, copyright 2021. (j) Schematic illustration of the interlayer spacing in $H_{11}Al_2V_6O_{23.2}$@Graphene. (k) Rate capability at 1–10 A g^{-1} and cycling performance at 2 A g^{-1} of HAVO@G with high areal loading. Reproduced from ref. 54 with permission from Springer, copyright 2019.

performance AZIBs. Despite the diverse design strategies developed for structural optimization, ion diffusion kinetics enhancement, and cycling stability improvement, both systems still suffer from issues such as capacity fading, limited rate capability, and challenges in practical implementation. Consequently, increasing attention has been directed toward another family of materials with distinctive layered structures and tunable electronic properties, transition metal dichalcogenides (TMDs). Two-dimensional layered TMDs typically exhibit a characteristic X–M–X configuration, where M denotes transition metals (*e.g.*, Mo, V, W, and Bi) and X corresponds to chalcogen elements such as S or Se (Fig. 7a). This stacked architecture facilitates charge carrier transport and accommodates volume variations during ion insertion/extraction. Moreover, owing to their compositional flexibility, structural diversity, and adjustable d-orbital electron occupancy, TMDs display a wide range of functional properties, spanning from insulators and semiconductors to superconductors.[79] Among them, molybdenum disulfide (MoS_2) has emerged as the most extensively studied representative. Its fundamental building unit consists of a molybdenum atomic layer sandwiched between two sulfur atomic layers, forming a "sandwich-like" structure. Strong covalent bonding dominates within the S–Mo–S layers, whereas adjacent layers are held together by van der Waals interactions.[80] Beyond its layered nature, MoS_2 exhibits polymorphism, including 1T, 2H, and 3R

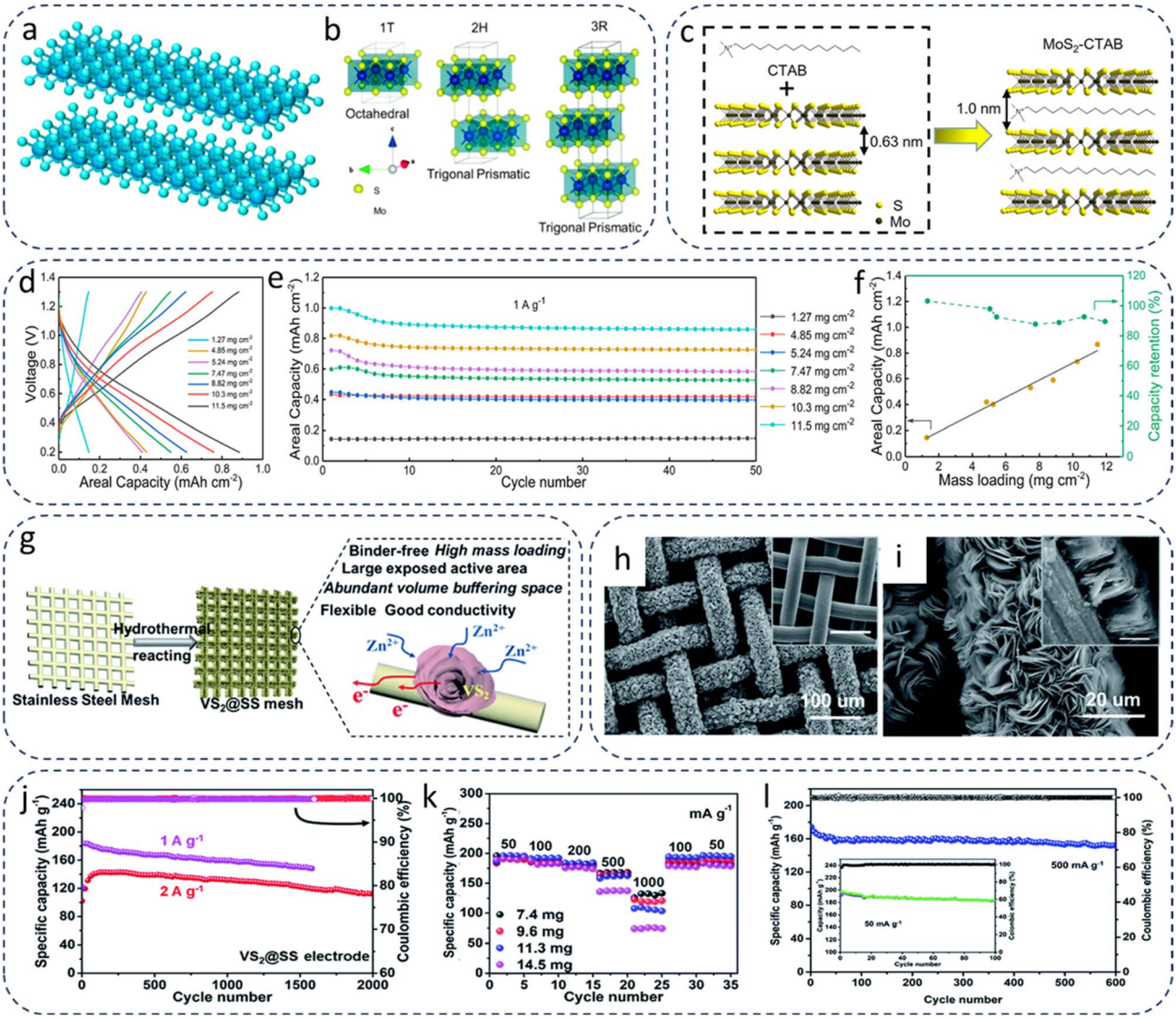

Fig. 7 (a) Illustration of the TMD structure. (b) Atomic structures of 1T-, 2H-, and 3R-MoS_2. Reproduced from ref. 83 with permission from MDPI, copyright 2022. (c) Schematic synthesis of the MoS_2-CTAB superlattice nanosheets and the *d*-spacing of the samples. Typical voltage curves (d) and areal capacities (e) of the MoS_2-CTAB electrode with different mass loadings at 1 A g^{-1} (5 C). (f) Areal capacity *vs.* areal mass loading and capacity retention at different areal loadings. Reproduced from ref. 22 with permission from American Chemical Society, copyright 2022. (g) Schematic illustration of the preparation processes for the binder-free hierarchical VS_2@SS electrode. (h) and (i) SEM image of VS_2 grown on a SS mesh. (j) Long-term cycling performance of the VS_2@SS electrode at 1 and 2 A g^{-1}. (k) Rate performances at different areal mass loadings. (l) Long-term cycling performances at 0.5 and 0.05 A g^{-1} (inset) with an areal loading of 11 mg cm^{-2}. Reproduced from ref. 57 with permission from The Royal Society of Chemistry, copyright 2019.

phases, each with distinct physicochemical characteristics (Fig. 7b). Specifically, both 2H- and 3R-MoS_2 feature Mo atoms in trigonal prismatic coordination, with the 2H phase stabilized by hexagonal symmetry stacking, while the 3R phase possesses rhombohedral symmetry containing three layers per unit cell.[81] In contrast, the 1T phase, which adopts an octahedral coordination for Mo atoms, is metallic in nature and the least stable. Besides MoS_2, vanadium disulfide (VS_2) is another representative TMD material, composed of alternating layers of sulfur and vanadium atoms stacked *via* van der Waals forces to form a sandwich-like structure.[82] At present, studies on TMDs in AZIBs remain at an early stage, and the reported high-loading cathode materials are largely confined to a few prototypes. Notably, MoS_2 and VS_2, with their unique interlayer architectures and promising electrochemical activity, have been among the first candidates explored and demonstrated as feasible options for high-loading AZIBs.

For example, Yao *et al.*[22] introduced a structural design concept based on volume regulation by developing a MoS_2/CTAB organic-inorganic superlattice electrode. By intercalating the flexible cationic surfactant CTAB into the rigid MoS_2 layers, the interlayer spacing was significantly expanded to 1.0 nm, while an ordered superlattice structure was simultaneously established (Fig. 7c). This architecture enabled Zn^{2+} ions to undergo in-plane expansion accompanied by synchronized interlayer contraction during intercalation, thereby achieving a "self-regulating volume" effect. Such a mechanism effectively alleviated the severe volume expansion and structural collapse commonly observed during Zn^{2+} insertion. As a result, the MoS_2-CTAB electrode not only exhibited remarkable rate performance and long-term cycling stability (92.8% capacity retention after 2100 cycles at 10 A g^{-1}), but also demonstrated considerable potential under high-mass-loading. When the active material loading was increased tenfold to approximately 11.5 mg cm^{-2}, the electrode still achieved an areal capacity of 0.87 mAh cm^{-2}, highlighting its significance for the design of thick electrodes and practical applications (Fig. 7d–f). In a complementary study, Jiao *et al.*[57] proposed a binder-free strategy to construct hierarchical VS_2 electrodes (Fig. 7g). Using a hydrothermal approach, 1T-phase VS_2 nanoflowers were directly grown *in situ* on stainless steel mesh, yielding a self-supporting VS_2@SS electrode (Fig. 7h and i). This configuration not only avoided the electrochemically inactive components associated with conventional binders and conductive additives, but also imparted a hierarchical porous architecture that improved electrolyte wettability and facilitated both electron and ion transport. At a typical mass loading of 4–5 mg cm^{-2}, the electrode delivered a specific capacity of 198 mAh g^{-1} and sustained over 2000 cycles (Fig. 7j). More importantly, under commercially relevant ultrahigh-mass-loading (~11 mg cm^{-2}), the electrode retained 90% of its capacity with a minimal decay rate of only 0.017% per cycle after 600 cycles, underscoring its excellent structural integrity and long-term cycling durability (Fig. 7k and l). This work clearly demonstrates that binder-free architectures combined with hierarchical array design can effectively overcome the ion transport and structural degradation bottlenecks typically encountered in thick electrodes under high-loading conditions.

Overall, transition metal sulfides represent a promising class of cathode materials for high-mass-loading AZIBs owing to their intrinsic layered structures, high electronic conductivity, and structural flexibility. These features facilitate efficient Zn^{2+} diffusion and help accommodate the stress associated with repeated intercalation under thick-electrode conditions. Recent advances in structural engineering, such as the construction of hierarchical architectures and interlayer modification, have further enhanced their electrochemical stability and capacity retention at commercially relevant loadings. Nevertheless, issues including interfacial stability, potential dissolution of sulfur species, and the scalability of synthesis routes remain key challenges. Continued efforts in interface regulation, composite design, and scalable fabrication are expected to further unlock the potential of transition metal sulfides in practical high-energy-density zinc-ion storage systems.

3.4 Other cathode materials

In addition to the widely investigated manganese oxides, vanadium-based compounds, and transition metal sulfides, manganese carbonate ($MnCO_3$) has recently been reported as a promising high-mass-loading cathode material for AZIBs. Owing to its natural abundance, low cost, and unique conversion reaction pathway, $MnCO_3$ can be electrochemically transformed into MnO_2 during cycling, thereby offering additional active sites for Zn^{2+} storage. For instance, $MnCO_3$ synthesized *via* a simple aqueous precipitation method exhibited a reversible capacity of 280 mAh g^{-1} at 50 mA g^{-1}.[59] Remarkably, even under a high-mass-loading of 7.2 mg cm^{-2}, the Zn–$MnCO_3$ cell maintained stable cycling for 2000 cycles, underscoring the feasibility of employing carbonate-type electrodes in thick-electrode configurations. This finding not only broadens the scope of manganese-based cathodes but also provides a new perspective on leveraging phase-transformation mechanisms to achieve high energy density and long cycle life under practical loading conditions.

4. Structure configuration

While the development of advanced electrode materials provides the foundation for improving the energy density and cycling stability of aqueous zinc-ion batteries under high-mass-loading conditions, material innovation alone is often insufficient to overcome the challenges of thick electrodes, such as sluggish ion transport, increased resistance, and structural degradation. To address these bottlenecks, a variety of structural and engineering strategies have been proposed to optimize electrode configuration and cell design. These approaches aim to improve electron/ion conductivity, enhance mechanical integrity, and maximize the utilization of active materials, thereby ensuring practical performance at commercially relevant loadings. In this section, we summarize five representative strategies, including conductive additive regulations, binder modifications, current collector regulation, free-standing structures, and 3D printing, highlighting their respective advantages and limitations (Table 3).

Table 3 Advantages and disadvantages of different structural and engineering strategies for high-mass-loading electrodes in AZIBs

Strategy	Advantages	Disadvantages
Conductive additive regulations	Enhances electron conductivity; improves rate performance; relatively simple to implement	Increases inactive weight/volume; excessive additives can reduce energy density
Binder modifications	Improves electrode mechanical stability; enhances adhesion to current collectors; can introduce ionic/electronic conductivity if functionalized	Some binders are electrochemically inactive or resist ion transport; potential side reactions
Current collector regulation	Provides robust electronic pathway; enables uniform current distribution; lightweight/porous collectors reduce inactive mass	Additional cost; limited compatibility with all electrode chemistries; potential corrosion in aqueous systems
Free-standing structures	Eliminates inactive binders and collectors; maximizes energy density; flexible and suitable for wearable devices	Fabrication can be complex; mechanical robustness under high loading may be limited
Three-dimensional printing	Enables precise control of electrode architecture; scalable for custom designs; allows rational tuning of porosity and loading	High cost; limited resolution for nanoscale features; still at an early research stage

4.1 Conductive additive regulations

Conductive additives constitute a cornerstone strategy for enabling practical, high-mass-loading cathodes in AZIBs. When electrode areal loading increases from the laboratory-typical few mg cm^{-2} toward practical values (>5–10 mg cm^{-2}), electronic percolation and interparticle contact become limiting factors: long electron pathways, localized electronic isolation of inner active particles, and enhanced polarization together reduce active material utilization and rate capability. Conductive additives remedy these deficiencies *via* three largely complementary roles: (i) establishing continuous electron-transport networks that connect interior particles to the current collector, (ii) improving the electrode microstructure (dispersion, pore architecture, and mechanical cohesion) so the electrolyte can penetrate and ions can reach internal sites, and (iii) providing interfacial functions (surface chemistry, protection against dissolution, and pseudocapacitive contribution) that stabilize electrochemistry under harsh, thick-electrode conditions.

Different classes of additives realize these roles by distinct mechanisms. Traditional carbon blacks and acetylene black principally serve as highly conductive, easily dispersed fillers to achieve percolation at low loadings, but they offer limited structural reinforcement and tend to aggregate in dense electrodes.[9,84] One- and two-dimensional carbons (CNTs, graphene, and rGO) combine high conductivity with anisotropic geometries, simultaneously forming percolating pathways and mechanically robust scaffolds.[29] Their high aspect ratio facilitates network formation at low weight fractions and helps maintain electrical contact even when electrodes crack during cycling. Conductive polymers (*e.g.*, PPy, PANI, and PEDOT) play dual roles as electronic conductors and conformal coatings.[19,36] By coating active particles or forming thin shells, they improve interfacial contact, suppress dissolution of active materials, and, in some instances, add reversible capacity owing to their redox activity. Finally, hybrid approaches that integrate conductive additives with architected electrode geometries (porous scaffolds, 3D printing, and free-standing films) are particularly effective for realizing simultaneously high areal capacity and fast kinetics in thick electrodes.[36]

Ma *et al.*[19] reported a vanadium nitride (VN) composite (Fig. 8a) with nitrogen-doped reduced graphene oxide (VN/N-rGO) in which N-rGO plays a dual role: (i) as a high-conductivity matrix that lowers charge-transfer resistance and (ii) as a structural binder that helps form a hierarchical porous network. Critically, the authors combined this composite strategy with material-extrusion 3D printing to fabricate electrodes with controlled macroporosity and tunable layer count (Fig. 8b); a three-layer printed electrode achieved 13 mg cm^{-2} mass loading while maintaining a high reversible specific capacity (390 mAh g^{-1}) and 89% retention after the initial activation cycles (Fig. 8c and d). The work explicitly shows that conductive-carbon integration plus deliberate macro-architecture can preserve ion and electron transport in electrodes that would otherwise suffer from severe underutilization. The printed porous pillars provide electrolyte channels and short ion diffusion distances within a thick electrode, while N-doped rGO improves wettability and charge transfer. A complementary example emphasizes the protective and dissolution-suppressing role of carbon coatings. Zhang *et al.*[54] prepared graphene-wrapped $H_{11}Al_2V_6O_{23.2}$ (HAVO@G) nanobelts: the thin graphene sheath increases electronic conductivity and limits vanadium dissolution in an aqueous electrolyte. Importantly for thick electrodes, the graphene wrapping allows the composite to retain structural integrity and charge accessibility even when the areal loading is pushed to ultrahigh values (~15.7 mg cm^{-2}). Under these conditions the electrode still delivered a reversible capacity of 131.7 mAh g^{-1} after 400 cycles at 2 A g^{-1} (Fig. 6k), demonstrating that an effective conductive coating can mitigate the typical tradeoff between loading and stability by maintaining electrical continuity and by acting as a physical barrier against dissolution. The study further reports that graphene wrapping reduces impedance growth at higher loadings, underscoring the value of intimate conductor–active interfaces in thick electrodes. The third exemplar spotlights conductive polymers as multifunctional additives. Qi *et al.*[15] introduced an *in situ* polypyrrole (PPy)

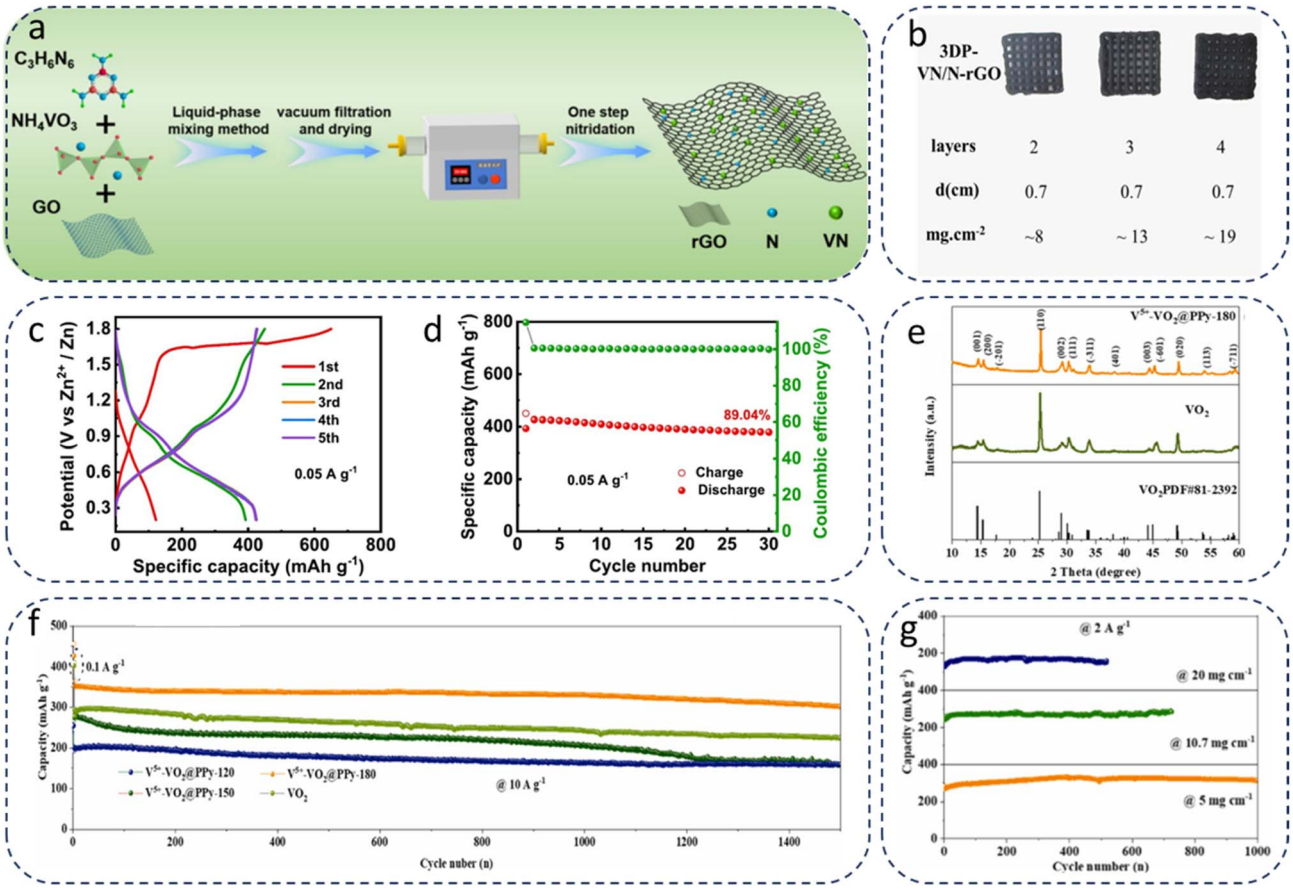

Fig. 8 (a) Schematic diagram of the preparation process of VN/N-rGO. (b) Photographs of 3DP-VN/N-rGO electrodes with different layers and varying mass loadings. (c) Discharge–charge curves and (d) cycling performance of the 3DP-VN/N-rGO electrode at 0.05 A g^{-1}. Reproduced from ref. 19 with permission from Elsevier, copyright 2025. (e) The XRD patterns of V^{5+}-VO_2@PPy and VO_2 materials. (f) The long-term cycle performance of four batteries at 10 A g^{-1} (Zn//V^{5+}-VO_2@PPy-1 20 150 180 and Zn//VO_2). (g) Cycle performance at 2 A g^{-1} based on various mass-loadings: 5, 10.7 and 20 mg cm^{-2}. Reproduced from ref. 15 with permission from Elsevier, copyright 2023.

coating on V^{5+}-rich VO_2 nanorods (V^{5+}-VO_2@PPy) (Fig. 8e). The thin PPy layer simultaneously increases electronic conductivity, forms a conformal protection against vanadium loss, and contributes to fast surface redox kinetics. As shown in Fig. 8f, this composite cathode demonstrates excellent rate capability (45.5 mAh g^{-1} at 10 A g^{-1}) and, importantly for practical applications, retains robust performance even at high-mass-loadings of up to 20 mg cm^{-2}, delivering 159.6 mAh g^{-1} over hundreds of cycles with minimal capacity decay (Fig. 8g). The PPy shell also stabilizes the mixed-valence VO_2 structure during cycling and helps preserve interfacial electron transport across the thick electrode. Thus, conductive polymer coatings can be a powerful solution where both transport and chemical stability (dissolution) are concerns.

For high-mass-loading cathodes, the regulation of conductive additives follows several key design principles:

(1) The inactive fraction should be minimized while still ensuring electronic percolation. High-aspect-ratio materials such as CNTs or graphene can achieve continuous networks at lower contents compared with conventional carbon blacks, thereby preserving both gravimetric and volumetric energy density.

(2) Additives should be integrated within hierarchical porous architectures, where macro- and meso-scale channels facilitate electrolyte penetration and shorten ion diffusion distances, while the conductive network guarantees electron transport.

(3) Conformal ultrathin coatings, such as carbon layers or conductive polymers, provide intimate contact between particles and the current collector while also suppressing active-material dissolution in aqueous electrolytes, thus improving long-term cycling stability at high loadings.

(4) Multifunctional additives are particularly attractive, as they not only enhance electronic conductivity but also reinforce electrode mechanics, improve electrolyte wettability, or contribute pseudocapacitive charge storage.

(5) Careful balance between additive amount, binder interactions, and electrode processing must be maintained, since excessive conductive fillers dilute the active mass and compromise overall energy density.

Despite the progress achieved through conductive-additive regulation, several challenges remain for high-mass-loading cathodes. First, the optimization of additive content is still difficult: insufficient amounts fail to establish continuous electronic pathways, while excessive additions dilute the active

material and reduce overall energy density. Second, maintaining a uniform dispersion of conductive additives within thick electrodes remains a practical bottleneck, as agglomeration or phase segregation can lead to uneven current distribution and localized polarization. Third, many conductive additives, especially polymers or surface-functionalized carbons, may suffer from chemical instability in aqueous electrolytes, causing performance decay over extended cycles. Finally, the compatibility of conductive additives with scalable electrode fabrication processes, such as slurry casting, roll-to-roll coating, or 3D printing, is yet to be fully demonstrated at industrially relevant scales. Future research should aim to design multifunctional conductive additives that combine high conductivity with structural reinforcement, dissolution suppression, and interfacial stability. The development of lightweight, high-aspect-ratio, and chemically robust conductive frameworks will be essential to minimize inactive mass while ensuring reliable performance. Moreover, integrating conductive-additive design with advanced electrode architectures (*e.g.*, graded porosity, self-supporting frameworks, or 3D-printed structures) is expected to further alleviate ion/electron transport bottlenecks under thick-electrode conditions.

4.2 Binder modifications

In the context of high-mass-loading cathodes for AZIBs, binder modification has emerged as a critical strategy to ensure electrode integrity and long-term electrochemical stability. Conventional polymeric binders such as polyvinylidene fluoride (PVDF) or carboxymethyl cellulose (CMC) are typically designed for low-loading electrodes, where mechanical stress and ion transport limitations are less pronounced.[60,85] However, under thick-electrode conditions, binders must perform multiple functions simultaneously: maintaining robust adhesion between active particles and the current collector, accommodating volume changes during Zn^{2+} insertion/extraction, and preserving electrode porosity to facilitate electrolyte penetration. To this end, researchers have explored advanced binders with tailored mechanical flexibility, ionic conductivity, and functional groups that enable strong chemical interactions with active materials. Conductive polymers (*e.g.*, polyaniline, polyacrylic acid: PAA, and PEDOT:PSS), bio-derived polymers (*e.g.*, alginate and chitosan), and hybrid binders incorporating inorganic nanoparticles have shown promise in reinforcing the electrode structure while contributing to charge transport.[86–88] Furthermore, binder engineering offers opportunities to reduce the reliance on conductive additives and inactive mass, which is particularly beneficial at high loadings. Functional binders incorporating polar groups (–COOH, –OH, and $–NH_2$) or conjugated structures can strengthen the adhesion between active particles and the current collector while simultaneously enhancing the electronic coupling across the electrode interface. Conductive or elastic binders further promote homogeneous charge distribution and accommodate mechanical deformation, thereby reducing interfacial resistance and prolonging cycling stability. Collectively, these structural engineering strategies synergistically improve the charge-transfer efficiency and durability of the electrode during long-term operation.

For instance, Zhou *et al.*[89] developed a multifunctional binder containing triazine rings and thiol groups *via* the nucleophilic ring-opening polymerization (ROP) of thiolactones with amine compounds (Fig. 9a). During charging, the thiol groups dynamically coordinate with Zn^{2+} ions, thereby facilitating ion transport, improving reaction kinetics, and enhancing both cycling stability and discharge capacity (Fig. 9b). The thiol-rich binder was processed together with electrolytic manganese dioxide (EMD) and a conductive additive to fabricate cathode sheets. Owing to the polar functional groups, the binder ensured strong adhesion between the active material and the current collector, while dynamic S–S bonds formed through thiol oxidation within the binder network further stabilized the cathode structure, leading to improved electrochemical performance. To assess the mechanical robustness of the synthesized binders, elastic modulus and hardness tests were conducted on different cathodes. As shown in Fig. 9c and d, the average modulus and hardness values of EMD/STN, EMD/SON, and EMD/SSN electrodes were significantly higher than those of EMD/PVDF, indicating a stronger resistance against volume change during cycling. Electrochemically, the EMD/STN cathode delivered an initial specific capacity of 123 mAh g^{-1} with a per-cycle fading rate as low as 0.033% over 500 cycles (Fig. 9e). Similarly, the EMD/SON and EMD/SSN cathodes exhibited initial capacities of 108 and 97 mAh g^{-1}, respectively, compared with only 68 mAh g^{-1} for the PVDF-based electrode. Polyacrylic acid has attracted considerable interest among various binders owing to its strong adhesion, ionic conductivity, and mechanical strength. However, its application in AZIBs has been constrained by the dissolution of transition metals during electrode processing with water-based solvents. To address this issue, Liu *et al.*[90] employed PAA dissolved in *N*-methyl-2-pyrrolidone (NMP), thereby suppressing transition-metal dissolution, and systematically investigated its role in high-mass-loading thick electrodes. As illustrated in Fig. 9f, the Zn^{2+} transport mechanism enabled by PAA can be described as follows: during charging, the –COOH groups partially dissociate into –COO– and H^+. The negatively charged –COO– moieties act as coordination sites for Zn^{2+}, facilitating ion migration, while the released H^+ combines with water molecules to form H_3O^+. Upon discharge, the –COO– groups recombine with H^+ to regenerate –COOH, simultaneously releasing Zn^{2+}. This dynamic process markedly lowers the migration barrier for Zn^{2+} ions. Moreover, the abundant hydrophilic –COOH groups in PAA reduce the electrode–electrolyte contact angle to 23.6° for $V_2O_5 \cdot nH_2O$-PAA electrodes, compared with 38.1° for hydrophobic PVDF-based counterparts. Improved wettability is beneficial for forming ion-conducting channels, thereby ensuring fast ion transport within the electrode. The stability imparted by PAA was further confirmed by soaking tests (Fig. 9g): the $V_2O_5 \cdot nH_2O$-PAA electrode exhibited minimal color change after several days, indicating effective suppression of vanadium dissolution. Importantly, at high current densities, the specific capacity of thick electrodes did not decrease significantly with increasing

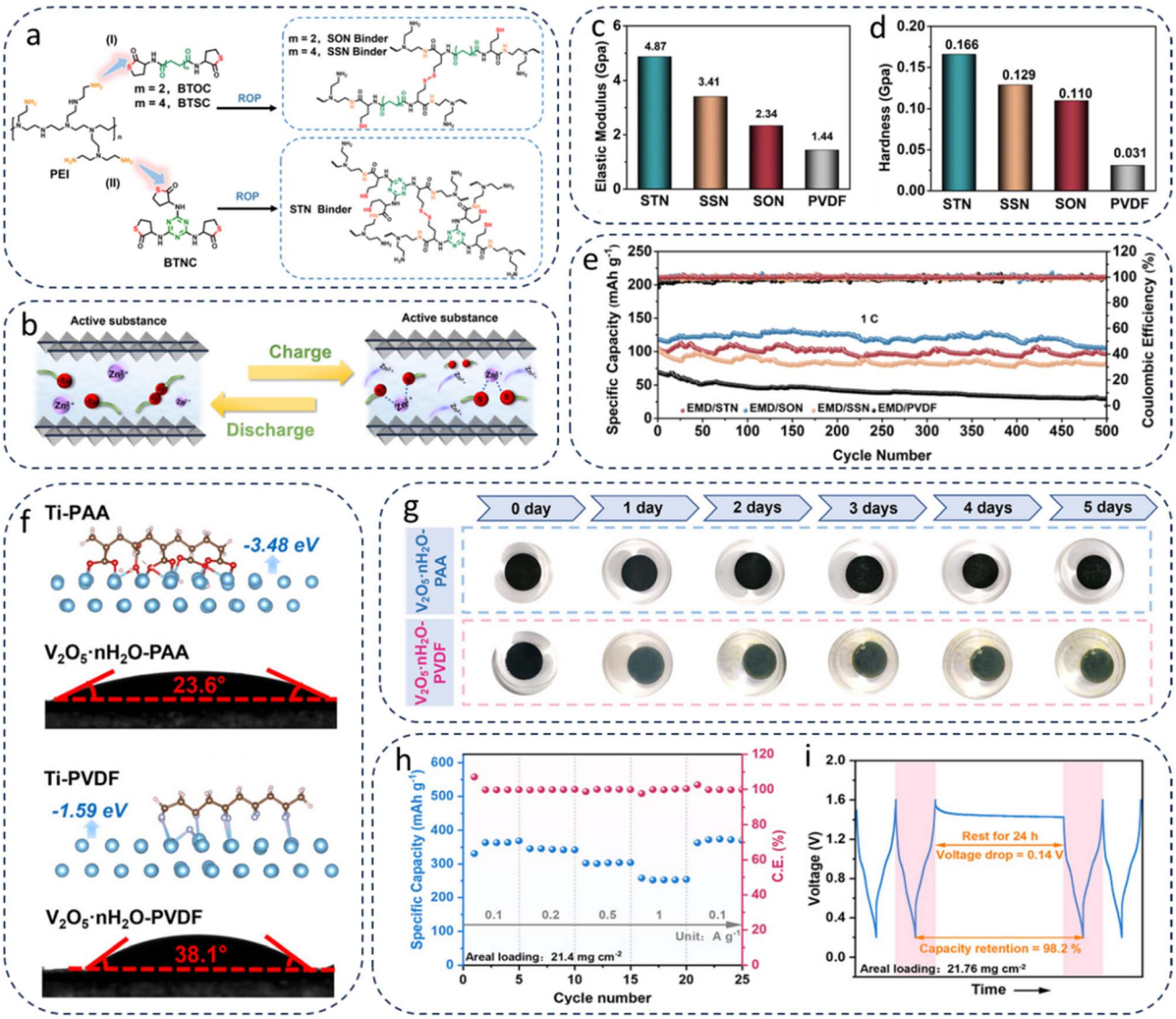

Fig. 9 (a) Schematic diagram of polymer binder synthesis. (b) Schematic diagram of binder action mechanism. (c) Elastic modulus of different cathodes. (d) Hardness of different cathodes. (e) Long-term cycling stability of different batteries at 1 C for 500 cycles. Reproduced from ref. 89 with permission from American Chemical Society, copyright 2025. (f) Binding structures of Ti with the PAA and PVDF binders and the contact angle of the electrodes with $Zn(CF_3SO_3)_2$ electrolyte. (g) Stability test of different electrodes soaked in 1 M $Zn(CF_3SO_3)_2$ electrolyte. Characterization of the thick $V_2O_5{\cdot}nH_2O$-PAA electrodes. (h) Rate performance. (i) Self-discharge test results. Reproduced from ref. 90 with permission from Wiley-VCH, copyright 2025.

mass loading, while the areal capacity increased linearly. Even at 1 A g^{-1}, the thick electrode maintained a capacity of 250 mAh g^{-1}, as shown in Fig. 9h. Furthermore, self-discharge tests on thick $V_2O_5{\cdot}nH_2O$-PAA electrodes demonstrated excellent stability: at a loading of 21.76 mg cm^{-2}, the voltage drop after 24 h was only 0.14 V, with a capacity retention of 98.2% and a loss of merely 1.8% (Fig. 9i). These results clearly verify that PAA binders can significantly enhance the charge–discharge performance and long-term stability of $V_2O_5{\cdot}nH_2O$ cathodes under high-mass-loading conditions.

Although binder modification offers significant potential for improving the electrochemical performance of high-mass-loading cathodes, several challenges remain. First, most conventional binders are electrochemically inert, meaning they do not contribute directly to capacity; thus, balancing the need for mechanical integrity with the minimization of inactive mass is still a critical issue. Second, ensuring uniform dispersion of binders within thick electrodes is difficult, and poor distribution often results in local mechanical failure, non-uniform ion transport, and uneven current distribution. Third, many functionalized or conductive binders, such as those based on conductive polymers, suffer from chemical instability in aqueous electrolytes or high-salt environments, leading to gradual performance degradation during long-term cycling. Moreover, the scalability of advanced binder systems remains underexplored, as many reported materials are developed at laboratory scale and may not yet be compatible with industrial roll-to-roll processing. To meet these challenges, a series of

design principles for binder modification have been proposed, which provide valuable guidance for the rational construction of high-performance thick electrodes. The key considerations can be summarized as follows:

(1) Binders should provide strong adhesion between active particles and the current collector while accommodating volume changes during cycling to prevent cracking and delamination.

(2) Advanced binders should maintain porous architectures for electrolyte penetration and may incorporate ionic or electronic conductive groups to reduce polarization and enhance charge transfer.

(3) Functional groups capable of coordinating with metal ions or active surfaces can improve cohesion, suppress dissolution, and enhance long-term electrochemical stability in aqueous environments.

(4) Binder content must be minimized to avoid excessive inactive mass, while eco-friendly, water-processable, and low-cost binders (*e.g.*, bio-derived polymers) are preferred for sustainable and industrial-scale electrode fabrication.

Next-generation binders should be multifunctional, combining strong adhesion with ionic/electronic conductivity, chemical stability, and structural flexibility. The incorporation of dynamic covalent bonds, supramolecular interactions, or self-healing functionalities could further enhance electrode resilience under repeated cycling. Bio-derived and water-soluble binders also offer sustainable and low-cost alternatives, aligning with the environmental advantages of AZIBs. In addition, binder engineering should be integrated with conductive additive optimization and electrode architecture design, ensuring synergy among all inactive components. Ultimately, rational binder modification will be crucial not only for enabling thick electrodes with high areal capacities, but also for facilitating the practical translation of AZIBs toward large-scale, long-lifetime energy storage systems.

4.3 Current collector regulation

In high-mass-loading cathodes for AZIBs, the current collector plays a decisive role in determining the electrode's overall conductivity, structural integrity, and electrochemical stability.[2,66] Conventional planar metal foil or meshes often fail to provide sufficient electron transport pathways and mechanical support when the electrode thickness increases, leading to uneven current distribution, high interfacial resistance, and limited utilization of active materials.[91] To address these challenges, the regulation of current collectors has emerged as an effective strategy to enhance the performance of thick electrodes. Approaches include tailoring the surface chemistry and morphology of traditional metal foils to improve adhesion and reduce contact resistance, employing lightweight porous substrates such as carbon cloth (CC), metal foams, or graphene frameworks to provide multidirectional electron channels and facilitate electrolyte penetration, and developing flexible or 3D structured collectors that combine conductivity with mechanical resilience.[76,92] These innovations not only enhance charge transport efficiency but also relieve stress accumulation during cycling, thereby enabling stable operation at high areal mass loadings. Overall, rational current collector design is indispensable for bridging the gap between high theoretical capacities of cathode materials and their practical deployment in thick-electrode AZIBs.

Carbon cloth has emerged as a promising flexible conductive substrate for supporting active materials, owing to its deformable interface that can effectively buffer structural strain. Integrating MnO_2 with conductive substrates can simultaneously enhance the electronic conductivity and mass loading of electrodes. Zheng *et al.*[92] employed a molecular manipulation strategy using CTAB nanomicelles to design a hierarchical micro/nano-structured MnO_2 self-supported CC electrode (denoted as MNSMO@CC) for AZIBs (Fig. 10a(i)). This nanomicelle-assisted method successfully promoted strong interfacial interactions at the MnO_2-CC interface, thereby generating an integrated electrode architecture. Moreover, the synergistic effect between the hierarchical MnO_2 structure and the CC substrate effectively alleviated the Jahn–Teller distortion of MnO_2 (Fig. 10a(ii and iii)). These results demonstrated that tailoring δ-MnO_2 on self-supporting collectors is a feasible route for achieving high-mass-loading electrodes. Accordingly, a high-MnO_2-loading MNSMO@CC electrode was fabricated. As shown in Fig. 10b, when the mass loading was increased to 6.1 mg cm^{-2}, the MNSMO@CC electrode delivered an areal capacity of 0.64 mAh cm^{-2} at 0.1 A g^{-1}, surpassing most previously reported MnO_2-based electrodes. Furthermore, at a loading of ~6.0 mg cm^{-2}, the electrode retained 81.8% of its capacity after 1300 cycles at 0.8 A g^{-1} (Fig. 10c). In addition, multiphysics simulations were conducted to elucidate the advantages of the MnO_2 structure during electrochemical reactions. At a current density of 1 mA cm^{-2}, the electric field simulation (Fig. 10d(i)) indicated that the highest potential was mainly localized near the CC substrate, with the field extending outward to the MnO_2 layer. This potential gradient facilitated directional electron transfer from the current collector to the active material. The charge distribution mapping (Fig. 10d(ii)) revealed that charges were predominantly concentrated on the coated MnO_2, while the strong electric field attracted Zn^{2+} ions toward the electrode interface, thereby improving the reaction kinetics of Zn^{2+} within the porous structure. The displacement cross-section (Fig. 10d(iii)) showed that deformation mainly occurred in the external MnO_2 layer, whereas the internal CC backbone experienced minimal strain. Moreover, the cross-sectional temperature distribution (Fig. 10d(iv)) remained uniform, supporting the thermal stability of the MNSMO@CC electrode during cycling. Collectively, these simulations highlighted that flexible CC can act as an elastic substrate to dissipate stress and provide robust mechanical integrity, while also enabling efficient electron/ion transport. This dual role renders CC an ideal platform for constructing high-mass-loading MnO_2 electrodes with enhanced electrochemical and structural stability. In addition, Ren *et al.*[51] employed alkali-treated carbon cloth as a current collector to support the *in situ* growth of 3D $Cu_{0.18}V_2O_5 \cdot 0.72H_2O$ nanostructures (denoted as CuVOH@CC) with the assistance of surfactants (Fig. 10e and f). This design was intended to achieve higher cathode mass loading and to address the issue of reduced specific capacity at elevated

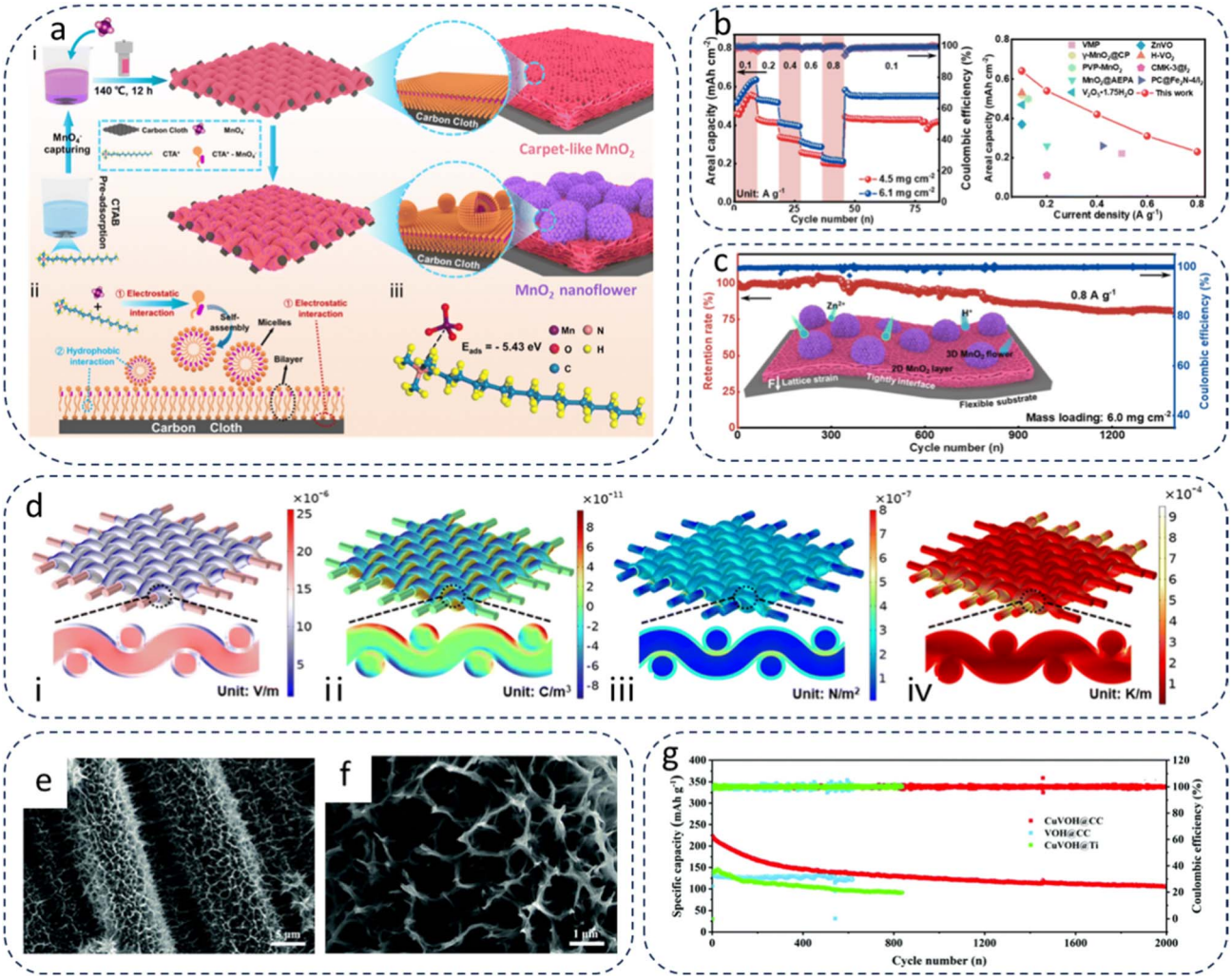

Fig. 10 (a) (i) The synthesis of MNSMO@CC, (ii) the molecular mechanism during the reaction, and (iii) the adsorption energy of the CTA^+-MnO_4^- molecule. (b) Rate performance and comparison of the areal capacity of the high-mass-loading MNSMO@CC electrode with that of previously reported electrodes. (c) Long-term cyclabilities of the Zn/MNSMO@CC batteries at 0.8 A g^{-1}. (d) COMSOL Multiphysics simulation of the (i) electric field, (ii) charge density distribution, (iii) structure deformation, and (iv) temperature difference of MnO_2@CC. Reproduced from ref. 92 with permission from Royal Society of Chemistry, copyright 2024. (e) and (f) SEM images of CuVOH@CC. (g) Long-term cycle performance at 1.0 A g^{-1} of CuVOH@CC and VOH@CC. Reproduced from ref. 51 with permission from Royal Society of Chemistry, copyright 2022.

loadings. By incorporating Cu^{2+} ions into the host lattice, whose ionic radius closely matches that of Zn^{2+}, the electrode exhibited enhanced rate capability and improved structural stability. At a mass loading of 7 mg cm^{-2}, the CuVOH@CC electrode delivered an initial specific capacity of 223.4 mAh g^{-1}, markedly higher than the 133.7 mAh g^{-1} of pristine VOH, and also demonstrated superior cycling stability (Fig. 10g). The development of such high-loading, high-capacity CuVOH@CC electrodes highlights the potential of AZIBs to move closer toward practical and industrial-scale implementation.

Despite notable advances, the regulation of current collectors in high-mass-loading AZIBs still faces several challenges. First, the balance between electronic conductivity and lightweight design remains a key bottleneck. Traditional metallic collectors (*e.g.*, stainless steel and titanium foil) provide excellent conductivity but significantly increase the inactive mass, thereby lowering the overall energy density. Conversely, lightweight alternatives such as carbon cloth or foams often suffer from limited conductivity or insufficient mechanical robustness under long-term cycling. Second, achieving strong interfacial adhesion between thick electrode coatings and current collectors is still difficult, particularly when the mass loading exceeds tens of mg cm^{-2}. Poor adhesion can lead to electrode delamination or loss of active material utilization during prolonged operation. Third, the fabrication of advanced porous or 3D-structured collectors often requires complex and costly synthesis processes, which hinders large-scale deployment. Maintaining uniformity of coating on such irregular surfaces is another challenge that must be addressed for industrial applicability. Therefore, design principles of current collector regulation in high-mass-loading AZIB cathodes are as follows:

(1) Surface modification techniques such as roughening, conductive coatings, or functional group introduction can

enhance adhesion between active materials and current collectors, reducing interfacial resistance and ensuring efficient charge transfer under high-mass-loading conditions.

(2) Constructing porous or hierarchical architectures on the current collector increases the surface area for active material deposition, facilitates electrolyte infiltration, and shortens ion/electron transport pathways in thick electrodes.

(3) Flexible substrates like carbon cloth or metal foams help accommodate volume changes during cycling, minimize mechanical failure, and preserve electrode integrity at high loading.

(4) Rationally engineered current collectors can provide chemical or electronic interactions with the active phase, thereby enhancing structural stability, conductivity, and long-term cycling performance in practical AZIBs.

Looking ahead, developing hybrid collectors that combine high conductivity with mechanical flexibility (*e.g.*, carbon-metal composites and graphene-coated foil) could mitigate trade-offs between conductivity, weight, and stability. Surface functionalization with polar or conductive coatings may also strengthen interfacial bonding and improve electrolyte wettability. In addition, scalable manufacturing techniques such as roll-to-roll coating, electrospinning, or additive manufacturing could help bridge the gap between laboratory-scale demonstrations and industrial implementation.

4.4 Free-standing structures

In high-mass-loading configurations, conventional slurry-cast electrodes typically require large amounts of conductive additives and polymeric binders to maintain structural stability and electron transport. However, these electrochemically inactive components inevitably reduce the overall energy density of the electrode, while thick electrodes often suffer from non-uniform ion diffusion and sluggish reaction kinetics.[93] To address these limitations, free-standing structures have emerged as a promising design strategy for AZIBs, especially under high-mass-loading conditions. Free-standing electrodes are generally constructed without the need for traditional current collectors or excessive binders, relying instead on the integrated assembly of active materials with conductive scaffolds to form a mechanically robust framework.[94] This approach not only maximizes the proportion of the electrochemically active material, thereby enhancing volumetric energy density, but also enables the creation of continuous 3D conductive networks that significantly improve ion/electron transport within thick electrodes. Specifically, free-standing electrodes are often fabricated by incorporating carbon-based scaffolds such as CNTs, graphene, CC, or carbon nanofibers, through techniques including *in situ* growth, vacuum filtration, or freeze-drying.[95,96] Such architectures offer several key advantages. First, their porous and interconnected networks greatly increase the electrode–electrolyte contact area, promoting electrolyte infiltration and facilitating fast ion migration, even at mass loadings exceeding 10 mg cm^{-2}. Second, the continuous conductive pathways ensure efficient electron transport throughout the thick electrode, mitigating resistance buildup associated with increasing thickness. Third, the inherent flexibility and mechanical robustness of free-standing structures help buffer volume expansion and contraction during cycling, preventing the pulverization and delamination of active materials, and thus preserving structural integrity over long-term operation. Beyond high loading, free-standing electrodes also demonstrate strong potential in flexible energy-storage devices. Their lightweight, flexible, and bendable characteristics make them particularly attractive for wearable or portable applications, where safety and mechanical resilience are essential.

For example, Zhang *et al.*[97] combined the functional characteristics of vanadium-based MOFs with electrospinning to fabricate a 3D free-standing VN embedded N-doped carbon nanofiber (VN/N-CNFs) composite with a hierarchical structure (Fig. 11a–c). During the thermal treatment, numerous whisker-like secondary nanostructures were hierarchically grown on the backbone carbon nanofibers, while uniformly distributed VN nanoparticles were *in situ* embedded within both the primary nanofibers and the branched whisker structures. The use of V-MOF enabled the homogeneous *in situ* distribution of active VN nanostructures within the carbon framework woven by electrospun nanofibers. This strategy not only suppressed the aggregation of zero-dimensional VN nanoparticles but also provided protective and conductive encapsulation, thereby minimizing direct exposure to aqueous electrolytes. As a result, the VN/N-CNFs cathode maintained a stable capacity of 482 mAh g^{-1} after 30 000 cycles at an ultrahigh current density of 50 A g^{-1} and still delivered 297 mAh g^{-1} even at 100 A g^{-1} (Fig. 11d and e). This work offers a new approach for designing electrodes with high capacity, high energy/power density, ultrafast charge/discharge capability, and exceptional cycle life for aqueous batteries. In another study, Wu *et al.*[78] fabricated a self-supporting, binder-free NaVO/MWCNTs electrode *via* a vacuum filtration process, with mass loadings ranging from 5.5 to 14.7 mg cm^{-2} (Fig. 11f). By optimizing the ratio of NaVO to MWCNTs, the electrode with a high loading of 14.7 mg cm^{-2} delivered an areal capacity of 3.2 mAh cm^{-2} at 0.5 A g^{-1}. Even at a high current density of 2 A g^{-1}, the NaVO/MWCNTs electrode exhibited both excellent rate performance and high areal capacity (Fig. 11g and h). Despite the large thickness typically associated with high-mass-loading electrodes, the NaVO/MWCNTs system maintained high utilization efficiency owing to its efficient electron/ion transport characteristics (Fig. 11i). Remarkably, the electrode demonstrated stable cycling performance and high coulombic efficiency over 1500 cycles, with a cumulative capacity output of 3.7 Ah cm^{-2} during the entire cycling test (Fig. 11j and k). These results highlight the significant practical potential of high-mass-loading NaVO/MWCNTs free-standing electrodes for advanced AZIB applications.

All in all, free-standing structures provide an effective route to overcome the limitations of traditional slurry-cast electrodes in high-mass-loading AZIBs. Nevertheless, despite their significant advantages in maximizing the proportion of the active material, enhancing ion/electron transport, and accommodating mechanical stress, several challenges remain that hinder their widespread implementation. One critical issue is the balance between high active material loading and structural integrity. Excessive loading can compromise the porosity of the

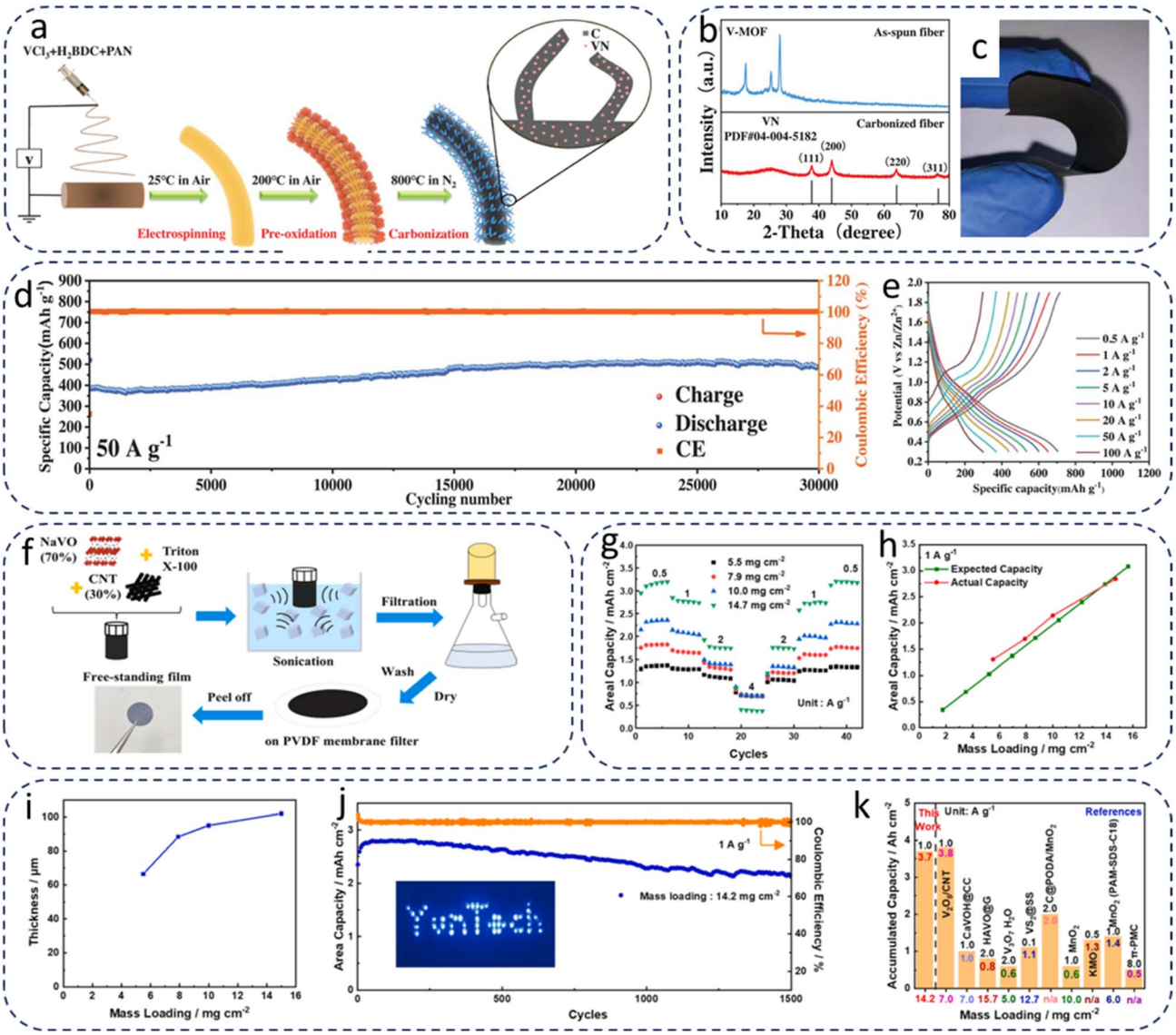

Fig. 11 (a) Schematic illustration of the synthesis procedures for the 3D self-supported hierarchical VN/N-CNFs skeleton. (b) XRD patterns of the as-spun nanofibril precursor and carbonized VN/N-CNFs composite. (c) Digital photo of the free-standing VN/N-CNFs membrane. (d) Long-term cycling performance at 50 A g^{-1} of self-supported VN/N-CNF cathodes. (e) Typical discharge/charge profiles at different current densities. Reproduced from ref. 97 with permission from Wiley-VCH, copyright 2022. (f) Schematic illustration of the procedures for obtaining self-supported NaVO/MWCNTs electrodes with high-mass-loading. (g) Rate performance, (h) the expected and actual areal capacities, and (i) thicknesses when loading different masses of NaVO/MWCNTs. (j) Cycle performance and (g) comparison of accumulated capacity of NaVO/MWCNTs and other reported cathodes. Reproduced from ref. 78 with permission from Elsevier, copyright 2024.

electrode, leading to limited electrolyte infiltration and sluggish ion kinetics. Another concern is the mechanical robustness of the free-standing framework, as repeated charge–discharge cycles may induce stress accumulation, structural collapse, or delamination, particularly in flexible configurations. Furthermore, many free-standing electrodes rely on sophisticated synthesis methods, such as *in situ* growth or advanced templating, which may pose obstacles for large-scale and cost-effective production. Finally, while free-standing structures show promise in combining high areal capacity with flexibility, there is often a trade-off between energy density, rate capability, and long-term stability that must be carefully addressed. Therefore, several practical design principles can be extracted for guiding the construction of free-standing electrodes under high-mass-loading conditions:

(1) Integrating conductive scaffolds such as carbon nanotubes, graphene, or carbon cloth with active materials can establish continuous conductive networks, ensuring efficient electron transport throughout the thick electrode.

(2) Creating hierarchical porosity and interconnected channels within the free-standing framework facilitates electrolyte infiltration and shortens ion diffusion pathways, which is critical for maintaining fast kinetics at high loadings.

(3) Mechanical flexibility and structural stability should be reinforced by employing robust scaffolding or flexible binders that buffer volume expansion and contraction during cycling.

(4) Multifunctional design approaches, such as incorporating heteroatom doping, polymer coatings, or hybrid structures, can simultaneously enhance conductivity, provide chemical stability, and suppress dissolution of active materials, thereby extending the cycle life of thick electrodes.

In summary, free-standing structures represent a powerful strategy to address the bottlenecks of high-mass-loading cathodes in AZIBs, offering advantages in terms of energy density, rate performance, and structural resilience. However, their practical application will depend on resolving challenges related to structural stability, scalability, and the trade-offs between different performance metrics. Future research should emphasize the rational integration of conductive scaffolds, the design of hierarchical and multifunctional architectures, and the development of scalable, low-cost fabrication techniques. By following these directions, free-standing electrodes are expected to bridge the gap between laboratory demonstrations and real-world applications, paving the way for high-energy-density and long-cycle-life zinc-ion batteries suitable for flexible and large-scale energy storage systems.

4.5 Three-dimensional printing

3D printing, also known as additive manufacturing, fabricates 3D objects through the layer-by-layer deposition of materials and has rapidly developed into a versatile manufacturing field.[98] Among the available techniques, material extrusion methods (such as direct ink writing (DIW) and fused filament fabrication) and vat photopolymerization approaches (including stereolithography and digital light processing, DLP) represent two of the most widely adopted categories.[98,99] 3D printing has recently emerged as a powerful tool for the design and fabrication of electrodes in AZIBs, particularly under high-mass-loading conditions where conventional methods often fall short.[100] Unlike slurry casting or vacuum filtration, which typically yield electrodes with limited structural control, 3D printing enables highly programmable and precise regulation of electrode geometry, porosity, and architecture at both the macro- and microscale.[21] This level of control is especially important for thick electrodes, where long ion diffusion paths and uneven reaction kinetics usually limit performance. By customizing electrode structures through computer-assisted design and additive manufacturing, researchers can tailor the internal arrangement of the active material and conductive frameworks to maximize utilization efficiency.[101] For example, optimized pore distributions can provide interconnected ion transport highways, while continuous conductive networks ensure efficient electron transfer across the entire electrode thickness.[102] From a structural perspective, 3D printing frameworks exhibit excellent mechanical robustness and structural integrity. The periodic lattice design can effectively distribute local stress and accommodate volumetric fluctuations during repeated Zn^{2+} insertion/extraction, preventing structural collapse or delamination. Furthermore, the printing process allows for rational material composition design, such as integrating conductive or elastic binders within the printed matrix, which simultaneously strengthens the electrode cohesion and improves interfacial stability. This capability directly addresses the transport heterogeneities and sluggish kinetics that are intrinsic to high-loading electrodes. In practical applications, 3D printing further offers several unique advantages.[102,103] First, it enables the rapid prototyping of complex and hierarchical electrode structures that would be difficult to achieve with conventional fabrication methods. Through the rational design of multi-scale porosity, 3D-printed electrodes allow sufficient electrolyte infiltration and homogeneous ion diffusion, thereby maintaining superior rate performance even at high areal capacities. Second, the formulation of printable inks that combine active materials with conductive additives and polymeric binders ensures a strong integration of electrochemical functionality with mechanical resilience. This integration not only enhances electrical conductivity but also improves structural robustness, effectively buffering the electrode against stress and volume variation during long-term cycling. Third, 3D printing is inherently scalable and adaptable. By adjusting printing parameters, layer thickness, or deposition patterns, it is possible to manufacture electrodes with customizable architectures that balance gravimetric, volumetric, and areal performance metrics. Moreover, the technique can be extended to fabricate flexible or even wearable electrodes, where mechanical adaptability is as important as electrochemical stability.

Nie *et al.*[17] developed a straightforward approach to fabricate high MnO_2 mass loading cathodes for AZIBs by integrating ultrasonic treatment, freeze-drying, and 3D printing techniques (Fig. 12a). In this strategy, commercially available materials were dispersed under ultrasonic processing to prepare printable inks, which were subsequently deposited as predesigned multilayer grid structures onto stainless steel substrates. After freeze-drying, grid-like cathodes with high MnO_2 mass loading were obtained, referred to as 3D cathodes. The mass loading of these electrodes could be conveniently adjusted by varying the number of printed layers (Fig. 12b). At an MnO2 mass loading of approximately 10 mg cm^{-2}, the 3D cathode delivered specific capacities of 251.5, 187.7, 127.8, 100.2, and 81.4 mAh g^{-1} at current densities of 0.1, 0.2, 0.5, 1, and 1.5 A g^{-1}, respectively. Even when the MnO_2 mass loading was increased to about 15 mg cm^{-2}, the electrode maintained excellent performance, achieving 113.3 mAh g^{-1} at 1 A g^{-1} and retaining 56.3 mAh g^{-1} after 400 cycles. As shown in Fig. 12c, Peng *et al.*[21] employed 3D printing to design and fabricate a high-mass-loading MnO_2 cathode with a mesh-like architecture (denoted as a 3D mesh MnO_2 cathode). For comparison, two control electrodes were prepared: one using the conventional slurry-coating method, and another fabricated by 3D printing but without the mesh structure (denoted as a 3D MnO_2 cathode). The flat and compact surface of the 3D MnO_2 cathode hindered electrolyte penetration into the interior of the electrode, thereby lowering the utilization of active material. In contrast, the mesh-like 3D MnO_2 electrode provided open ion transport channels, facilitating electrolyte storage and rapid ion diffusion. Its interconnected framework ensured sufficient contact between the electrolyte and the electrode, thereby offering abundant electrochemically active sites for reactions (Fig. 12d). The layer-by-

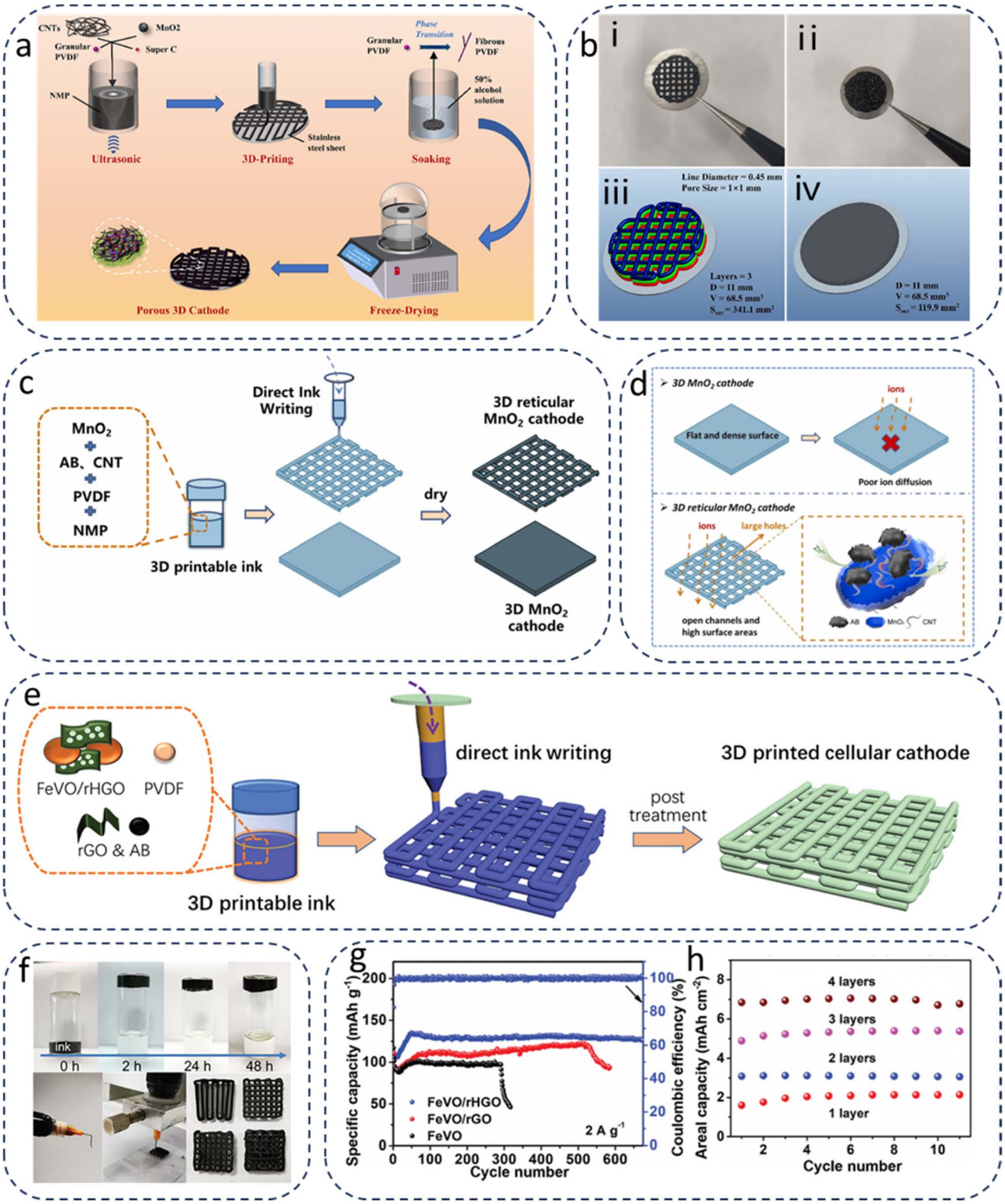

Fig. 12 (a) Schematic illustration of the fabrication process of a high MnO_2 mass loading 3D cathode. (b) (i) Optical image of a 3D cathode, (ii) optical image of a BC cathode, (iii) model image of a 3D cathode, and (iv) model image of a BC cathode. Reproduced from ref. 17 with permission from Elsevier, copyright 2023. (c) 3D printing process diagram of a 3D reticular MnO_2 cathode and 3D MnO_2 cathode. (d) Schematic diagram of ion transmission of 3D MnO_2 and 3D reticular MnO_2. Reproduced from ref. 21 with permission from Elsevier, copyright 2024. (e) Schematic of DIW-based fabrication of cellular FeVO/rHGO cathodes for AZIBs. (f) Photographs of printable ink, a printing syringe, and printed patterns with different layers. (g) Long-term cycling performance at a current density of 2 A g^{-1}. (f) Areal capacities of 3DP-FeVO/rHGO with different printing layers at a current density of 6 mA cm^{-2}. Reproduced from ref. 55 with permission from Wiley-VCH, copyright 2024.

layer deposition enabled by 3D printing allowed the MnO_2 cathode to be fabricated in a self-supporting configuration without the need for a current collector, which further enhanced mass loading and consequently improved areal capacity. As a result, AZIBs assembled with a double-layer 3D mesh MnO_2 cathode achieved a high areal capacity of 2.84 mAh cm^{-2} even at an ultrahigh current density of 10 mA cm^{-2}. Moreover, Ma *et al.*[55] explored a DIW approach to fabricate high-mass-loading honeycomb-like cathodes for AZIBs, with the DIW printing process illustrated in Fig. 12e. Notably, this unique DIW technique allowed the electrode structure to be readily configured into a honeycomb architecture, while its internal chemical composition could also be tuned. One of the most critical challenges in constructing 3D-printed electrodes lies in developing printable inks with appropriate rheological behavior and optimized formulations. As shown in Fig. 12f, when an inverted vial containing the prepared ink was left for 48 hours, the ink at the bottom did not flow along the wall, indicating its excellent self-supporting ability. At the same time, the continuous extrusion of the ink demonstrated favorable flow characteristics. By simply adjusting the printing path, honeycomb electrodes with different layer numbers could be manufactured without altering the overall structure. The 3D-printed cathodes with mass loadings exceeding 10 mg cm^{-2} exhibited remarkable cycling stability, sustaining more than 650 cycles at 2 A g^{-1} (Fig. 12g). Furthermore, the mass loading could be readily increased to 24.4 mg cm^{-2} using this printing strategy, thereby delivering an ultrahigh areal capacity of 7.04 mAh cm^{-2} (Fig. 12h).

In conclusion, 3D printing has demonstrated clear advantages in the fabrication of high-mass-loading electrodes for AZIBs, offering precise structural control, tunable porosity, and scalable customization. However, its current application is still accompanied by notable limitations. A major challenge lies in the development of printable inks that simultaneously meet rheological requirements for extrusion or photopolymerization while preserving electrochemical activity. Many inks suffer from issues such as sedimentation, agglomeration of active particles, or poor mechanical stability once printed. In addition, the printing resolution and structural fidelity remain insufficient for producing fine micro-to nanoscale architectures that are crucial for fast ion transport in thick electrodes. Another limitation is the mechanical robustness of printed electrodes, which may degrade over extended cycling due to stress accumulation, fracture, or loss of structural integrity. Furthermore, the relatively high cost and slow printing rates of current 3D technologies constrain their feasibility for large-scale and industrial production. From these insights, several design principles can be utilized for future applications of 3D printing in AZIB cathodes:

(1) Optimizing ink formulation is essential, where the combination of active materials, conductive additives, and binders must achieve balanced rheological properties, structural stability, and electrochemical functionality.

(2) Hierarchical structural design should be pursued, integrating macro-porous channels for electrolyte infiltration with micro/nanostructured domains to ensure efficient ion/electron transport at high loading.

(3) Multifunctionality should be embedded into the printed structures by incorporating conductive or protective components that can simultaneously enhance conductivity, mechanical strength, and chemical stability.

(4) Scalability and cost-effectiveness need to be addressed by developing rapid printing processes and low-cost precursor materials, ensuring that the advantages of 3D printing can extend beyond laboratory-scale demonstrations toward industrial applications.

Looking ahead, the integration of 3D printing into AZIB electrode design is expected to evolve from proof-of-concept demonstrations toward more practical and scalable applications. Future research should focus on the rational development of multifunctional printable inks that couple high electrochemical activity with mechanical resilience and processing stability. At the same time, efforts should be directed toward improving the resolution and speed of printing techniques to enable the fabrication of electrodes with precisely engineered hierarchical architectures on a large scale. Combining 3D printing with emerging strategies such as digital design, artificial intelligence-assisted optimization, and green manufacturing could further enhance both performance and sustainability. Ultimately, 3D printing has the potential to bridge the gap between structural innovation and industrial feasibility, providing a versatile platform for constructing next-generation high-mass-loading AZIB electrodes with high energy density, robust cycling stability, and adaptability to flexible or customized energy storage devices.

5. Conclusion and perspectives

Aqueous zinc-ion batteries (AZIBs) have emerged as a promising candidate for next-generation large-scale energy storage due to their intrinsic safety, low cost, and environmental compatibility. However, translating AZIBs from laboratory-scale studies to practical applications requires the realization of cathodes with high mass loading, which directly determines the attainable areal capacity and overall energy density. In this review, we systematically summarized recent advances in cathode materials and structural engineering strategies that enable high-mass-loading electrode designs. The discussions encompass manganese-based oxides, vanadium-based compounds (including V_2O_5, metal vanadates, and other derivatives), transition metal sulfides, as well as alternative systems such as $MnCO_3$. Moreover, diverse engineering approaches such as conductive additive regulation, binder optimization, current collector modification, free-standing architectures, and three-dimensional (3D) printing have been explored to address the limitations associated with thick electrodes.

On the materials side, Mn-based oxides remain attractive due to their abundance and multiple redox states, with progress achieved through nanostructuring, defect engineering, and heteroatom doping to mitigate sluggish kinetics under high mass loading. Vanadium-based systems offer high theoretical capacities and versatile structural tunability. In particular,

alkaline-earth metal vanadates (*e.g.*, Ca-, Mg- and Ba-based) demonstrate the "pillar effect," stabilizing layered frameworks and supporting high areal capacities at practical loadings. Alkali-metal vanadates such as $K_{0.486}V_2O_5$ and $Na_xV_2O_5 \cdot nH_2O$ highlight the importance of electrolyte regulation and flexible electrode design, showing encouraging results in thick electrodes and quasi-solid-state configurations. Other vanadium-based compounds including VO_2, $V_3O_7 \cdot H_2O$, and hydrated derivatives broaden the materials landscape, whereas transition metal sulfides such as MoS_2 and VS_2 benefit from high conductivity and layered diffusion channels. Furthermore, $MnCO_3$, with its *in situ* transformation to MnO_2, exemplifies the potential of unconventional cathodes to deliver stable cycling under elevated mass loading.

While high-loading cathodes hold the key to improving the energy density of AZIBs, their practical implementation inevitably imposes additional demands on both the anode and the electrolyte. On the anode side, the intensified Zn^{2+} fluxes and locally fluctuating electric fields under high cathode loadings can aggravate uneven Zn deposition, dendritic growth, and by-product accumulation. Such effects not only undermine the reversibility of Zn plating/stripping but also accelerate corrosion and hydrogen evolution, leading to gradual polarization buildup and shortened cycle life. Addressing these issues requires careful regulation of Zn utilization and interfacial stability. Promising approaches include employing surface-modified Zn foil, constructing artificial solid-electrolyte interphases, or introducing 3D structured hosts that can homogenize ion flux and mitigate local stress during cycling. The electrolyte likewise plays a decisive role in sustaining stable operation under high-loading conditions. Concentrated or hybrid electrolytes with tailored Zn^{2+} solvation structures have shown the ability to suppress parasitic reactions and enhance Zn reversibility, while gel or solid-state formulations can further improve mechanical stability and interfacial compatibility. Moreover, the optimization of ionic conductivity, buffering capability, and additive chemistry must be balanced with manufacturability and cost considerations to ensure practical viability. In future developments, a more integrated design that simultaneously considers cathode, anode, and electrolyte interactions will be essential to unlock the full potential of high-mass-loading AZIBs.

Beyond material innovation, structural strategies are equally crucial for practical electrode designs. Conductive additives with high aspect ratios and multifunctional properties form efficient percolation networks while minimizing inactive content. Advanced binders with strong adhesion, ionic conductivity, and dynamic bonding (*e.g.*, PAA and functionalized polymers) enhance electrode integrity and facilitate Zn^{2+} transport. Tailored current collectors such as carbon cloth or surface-modified substrates not only support mechanical stability but also improve charge transfer in thick electrodes. Free-standing architectures eliminate the need for binders and collectors, significantly increasing the active material ratio, while modified separators regulate ion transport and suppress parasitic reactions. Notably, 3D printing offers unprecedented control over electrode architecture, enabling hierarchical porosity, scalable fabrication, and integration of mechanical robustness with electrochemical performance, making it an emerging platform for future industrialization.

Despite these encouraging advances, challenges remain. At high-mass-loading, issues such as sluggish ion/electron transport, mechanical stress, electrolyte saturation, and structural degradation continue to limit long-term stability. Moreover, the balance between gravimetric capacity, areal capacity, and volumetric energy density needs to be carefully managed to meet application-specific requirements. From a practical standpoint, scalable synthesis methods, cost-effective electrode fabrication, and compatibility with pouch-cell or flexible-device configurations are essential for translating laboratory findings into real-world energy storage systems. Looking forward, several promising research directions can be envisioned to further advance the development of high-mass-loading AZIBs.

(1) Material innovation should be coupled with structural engineering in a holistic manner. While substantial progress has been achieved in modifying individual material properties such as conductivity or stability, the next stage requires integrating multiple strategies within a single electrode system. For instance, simultaneously introducing heteroatom doping, layered ion-pillaring, and hybrid conductive scaffolds could provide synergistic improvements in Zn^{2+} diffusion kinetics, structural robustness, and electrochemical utilization. Moreover, multi-component composites that combine transition-metal oxides, sulfides, or conductive polymers with carbonaceous networks may deliver multifunctionality, balancing the trade-offs between energy density, power density, and cycle life under high areal loading.

(2) Advanced manufacturing and scalable processing technologies must be prioritized. Although impressive areal capacities have been demonstrated under well-controlled laboratory conditions, large-scale production demands fabrication methods that are low-cost, scalable, and highly reproducible. The development of printable inks or slurries with controlled rheology and optimized conductive/binder networks will be particularly important for enabling industrial-scale production of high-mass-loading electrodes without compromising structural precision or electrochemical performance. In practical cell configurations, thick electrodes often suffer from limited ion diffusion and increased internal resistance, leading to performance degradation. Rational design of porous and conductive frameworks, coupled with scalable fabrication routes, could overcome these issues by enabling efficient electrolyte penetration and mechanical robustness. In addition, the integration of advanced electrode designs with industrial-scale coating and lamination technologies (*e.g.*, roll-to-roll or slot-die coating) may accelerate the transition from lab-scale coin cells to pouch-type or flexible Zn-ion devices. Future research should also address electrolyte optimization, interface engineering, and mechanical reliability under high areal capacity and high current density conditions.

(3) In-depth mechanistic understanding through advanced characterization is indispensable. High-loading electrodes exhibit complex behaviors such as inhomogeneous ion distribution, localized stress accumulation, and dynamic phase

transitions, which are difficult to capture using conventional *ex situ* methods. Therefore, *operando* and *in situ* techniques (*e.g.*, X-ray diffraction, synchrotron-based spectroscopy, cryo-electron microscopy, and neutron scattering) should be widely applied to monitor the real-time evolution of cathode structures during cycling. Coupling these insights with theoretical modeling and computational simulations, including density functional theory (DFT) and finite-element analysis, will provide mechanistic guidance for rational electrode and electrolyte designs.

(4) Long-term reliability, safety, and sustainability must be addressed for real-world applications. While many high-mass-loading cathodes demonstrate impressive laboratory performance, practical conditions such as large-format pouch cells, variable temperature, and mechanical deformation can introduce new challenges. Future work should systematically evaluate failure modes of thick electrodes, including gas evolution, electrode delamination, and electrolyte dry-out, under realistic operating scenarios. At the same time, the development of sustainable precursors, environmentally benign processing, and recyclable materials will align the technology with green and cost-effective energy storage demands.

(5) Interdisciplinary approaches that combine materials science, electrochemistry, and data-driven methods will accelerate progress. Machine learning and artificial intelligence can assist in predicting optimal electrode architectures, binder formulations, or electrolyte compositions based on large datasets, thus shortening the discovery cycle. Integrating computational design, automated synthesis, and high-throughput screening platforms could revolutionize the way high-mass-loading AZIBs are developed, ultimately paving the way for industrial implementation.

In conclusion, while considerable challenges remain, the convergence of materials innovation, structural engineering, electrolyte optimization, scalable manufacturing, and advanced characterization is expected to establish a robust foundation for the next generation of AZIBs. With these concerted efforts, high-mass-loading cathodes can transition from academic demonstrations to practical, durable, and safe energy storage solutions, enabling wide-ranging applications from grid-scale renewable integration to portable and flexible electronics.

Author contributions

Y. Ran drafted the initial version of the manuscript. H. P. Zhao reviewed and refined the initial draft. Y. Lei provided overall guidance, reviewed the initial draft, and handled the submission process. All authors contributed to the discussion of results and approved the final manuscript.

Conflicts of interest

There are no conflicts to declare.

Data availability

No primary research data, software, or code were included, and no new data were generated or analysed in this review.

Acknowledgements

The authors acknowledge support from the German Research Foundation (DFG, Project number 501766751) and the Sino-German Center for Research Promotion (GZ1579). Yan Ran would like to appreciate the support from the China Scholarship Council (No. 202207030010).

Notes and references

1 Z. Y. Fan, J. W. Wang, Y. P. Wu, X. D. Yan, D. M. Dai and X. L. Wu, *J. Energy Chem.*, 2024, **97**, 237–264.
2 Y. H. Xu, G. N. Zhang, J. Q. Liu, J. H. Zhang, X. X. Wang, X. H. Pu, J. J. Wang, C. Yan, Y. Y. Cao, H. J. Yang, W. B. Li and X. F. Li, *Energy Environ. Mater.*, 2023, **6**, e12575.
3 Y. Ran, J. Ren, Y. Kong, B. Wang, X. Xiao and Y. Wang, *Electrochim. Acta*, 2022, **412**, 140120.
4 C. Guo, S. J. Yi, R. Si, B. J. Xi, X. G. An, J. Liu, J. F. Li and S. L. Xiong, *Adv. Energy Mater.*, 2022, **12**, 2202039.
5 X. Geng, X. Hou, X. He and H. J. Fan, *Adv. Energy Mater.*, 2024, **14**, 2304094.
6 Y. Li, Z. H. Wang, Y. Cai, M. E. Pam, Y. K. Yang, D. H. Zhang, Y. Wang and S. Z. Huang, *Energy Environ. Mater.*, 2022, **5**, 823–851.
7 M. Y. Ye, Y. Y. Guan, R. Xu, P. F. Wang, Y. H. Zhang, J. Yu, D. P. Li, L. Li, Q. Zhao, Z. J. Wang, J. Y. Liang and Y. H. Wu, *J. Energy Chem.*, 2025, **106**, 650–670.
8 M. Chen, S. C. Zhang, Z. G. Zou, S. L. Zhong, W. Q. Ling, J. Geng, F. A. Liang, X. X. Peng, Y. Gao and F. G. Yu, *Rare Met.*, 2023, **42**, 2868–2905.
9 Y. Ran, F. Dong, S. Sun and Y. Lei, *Adv. Energy Mater.*, 2025, 2406139.
10 Y. Ran, M. Y. Li, H. P. Zhao, J. Ren, Y. L. Sheng, G. S. Shao, Y. D. Wang and Y. Lei, *Adv. Funct. Mater.*, 2025, e10241.
11 H. T. Xu, W. Y. Yang, M. Li, H. B. Liu, S. Q. Gong, F. Zhao, C. L. Li, J. J. Qi, H. H. Wang, W. C. Peng and J. P. Liu, *Small*, 2024, **20**, 2310972.
12 G. J. Li, L. Sun, S. L. Zhang, C. F. Zhang, H. Y. Jin, K. Davey, G. M. Liang, S. L. Liu, J. F. Mao and Z. P. Guo, *Adv. Funct. Mater.*, 2024, **34**, 2301291.
13 Y. Ran, J. Ren, Z. C. Yang, H. Zhao, Y. Wang and Y. Lei, *Small Struct.*, 2023, **4**, 2300136.
14 L. Yang, Y. J. Zhu, F. L. Zeng, L. Y. Dong, J. C. Tao, G. He and H. Li, *Energy Storage Mater.*, 2024, **65**, 103162.
15 Y. Qi, X. Q. Jin, L. Xu, X. F. Ren and Y. Y. Xia, *J. Alloys Compd.*, 2023, **967**, 171750.
16 P. Shang, Y. H. Liu, Y. Y. Mei, L. S. Wu and Y. F. Dong, *Mater. Chem. Front.*, 2021, **5**, 8002–8009.
17 N. T. Nie, F. L. Wang and W. H. Yao, *Electrochim. Acta*, 2023, **472**, 174772.
18 D. Chen, M. J. Lu, B. R. Wang, H. F. Cheng, H. Yang, D. Cai, W. Han and H. J. Fan, *Nano Energy*, 2021, **83**, 105835.
19 H. Ma, C. Y. Tang, F. W. Zhang, Z. Q. Tao, J. H. Liu, B. Yan and H. C. Tao, *Appl. Surf. Sci.*, 2025, **710**, 163917.
20 G. Nam, C. Hwang, H. Jang, N. Kane, Y. Ahn, M. J. Kwak, Z. Y. Luo, T. T. Li, M. G. Kim, N. Liu and M. Liu, *Small*, 2024, **20**, 2306919.

21 J. Peng, W. S. Gou, T. Jiang, K. P. Ding, A. Y. Yu, Q. Fan and Q. Y. Xu, *J. Alloys Compd.*, 2024, **998**, 174772.
22 Z. Y. Yao, W. Zhang, X. C. Ren, Y. R. Yin, Y. X. Zhao, Z. G. Ren, Y. H. Sun, Q. Lei, J. Wang, L. H. Wang, T. Ji, P. Huai, W. Wen, X. L. Li, D. M. Zhu and R. Z. Tai, *Acs Nano*, 2022, **16**, 12095–12106.
23 K. Fang, Y. L. Liu, P. Chen, H. Zhang, D. L. Fang, H. Y. Zhang, Z. Wei, L. Ding, G. G. Wang and H. Y. Yang, *Nano Energy*, 2023, **114**, 108671.
24 T. T. Lv, Y. Peng, G. X. Zhang, S. Jiang, Z. L. Yang, S. Y. Yang and H. Pang, *Adv. Sci.*, 2023, **10**, 2206907.
25 L. Fan, Y. Ru, H. G. Xue, H. Pang and Q. Xu, *Adv. Sustain. Syst.*, 2020, **4**, 2000178.
26 W. K. Jiang, K. Y. Zhu and W. S. Yang, *Chem.–Eur. J.*, 2023, **29**, e202301769.
27 Y. X. Guo, Y. X. Zhang and H. B. Lu, *Battery Energy*, 2022, **1**, 20210014.
28 B. Zhang, P. Dong, S. Y. Yuan, Y. N. Zhang, Y. J. Zhang and Y. G. Wang, *Chem. Bio Eng.*, 2024, **1**, 113–132.
29 H. Yang, Y. Wan, K. Sun, M. D. Zhang, C. Z. Wang, Z. Q. He, Q. Li, N. Wang, Y. L. Zhang, H. Hu and M. B. Wu, *Adv. Funct. Mater.*, 2023, **33**, 2215076.
30 S. Z. Deng, B. A. Xu, X. L. Liu, C. W. Kan and T. D. Chen, *Chem.–Eng. J.*, 2023, **475**, 146098.
31 P. Shang, Y. H. Liu, Y. Y. Mei, L. S. Wu and Y. F. Dong, *Mater. Chem. Front.*, 2021, **5**, 8002–8009.
32 M. J. Shi, B. Wang, C. Chen, J. W. Lang, C. Yan and X. B. Yan, *J. Mater. Chem. A*, 2020, **8**, 24635–24644.
33 Y. Liu, J. Zhi, T. K. A. Hoang, M. Zhou, M. Han, Y. Wu, Q. Y. Shi, R. Xing and P. Chen, *Acs Appl. Energ. Mater.*, 2022, **5**, 4840–4849.
34 L. J. Chen, Y. Y. Dong, M. W. Han, T. Song, X. J. Zheng, W. Y. He, B. Long, X. W. Wu, Y. Pei and X. Y. Wang, *Chem.–Eng. J.*, 2023, **473**, 145046.
35 H. F. Jia, Y. X. Li, L. H. Fu, U. Ali, B. Q. Liu, L. Y. Zhang, H. Z. Wang, L. Li, H. G. Wang and C. A. Wang, *Small*, 2023, **19**, 2303593.
36 L. W. Ma, W. Y. Xinyu and J. C. Sun, *J. Electroanal. Chem.*, 2020, **873**, 114395.
37 X. F. Li, L. Y. Yang, H. Y. Mi, H. Z. Li, M. Zhang, A. Abliz, F. J. Zhao, S. Y. Wang and H. B. Li, *Crystengcomm*, 2021, **23**, 8650–8659.
38 Q. Pan, R. Dong, H. Z. Lv, X. Q. Sun, Y. Song and X. X. Liu, *Chem.–Eng. J.*, 2021, **419**, 129491.
39 D. Y. Zhao, X. Y. Wang, W. M. Zhang, Y. J. Zhang, Y. Lei, X. T. Huang, Q. C. Zhu and J. P. Liu, *Adv. Funct. Mater.*, 2023, **33**, 2211412.
40 J. J. Sun, Y. F. Zhao, Y. Y. Liu, H. M. Jiang, C. Huang, M. Cui, T. Hu, C. G. Meng and Y. F. Zhang, *Small Struct.*, 2022, **3**, 2100212.
41 T. Y. Wei, Q. Li, G. Z. Yang and C. X. Wang, *Adv. Energy Mater.*, 2019, **9**, 1901480.
42 D. Chen, M. J. Lu, B. R. Wang, H. F. Cheng, H. Yang, D. Cai, W. Han and H. J. Fan, *Nano Energy*, 2021, **83**, 12345.
43 S. Y. Li, B. Lv, J. Gao, X. R. He and J. Wang, *J. Alloys Compd.*, 2025, **1021**, 179721.
44 S. Linghu, J. H. Ye, K. Deng, P. Liu, Y. Zhong, T. You, W. Tian, J. Y. Ji and J. Power, *Sources*, 2024, **592**, 233922.
45 Y. H. Du, X. Y. Wang, Y. Zhang, H. B. Zhang, J. Z. Man, K. Liu and J. C. Sun, *Chem.–Eng. J.*, 2022, **434**, 134642.
46 Y. Jiang, J. Lu, W. Liu, C. Xing, S. Y. Lu, X. Y. Liu, Y. Xu, J. J. Zhang and B. Zhao, *Acs Appl. Mater. Inter.*, 2022, **14**, 17415–17425.
47 F. J. Tang, W. J. Zhou, M. F. Chen, J. Z. Chen and J. L. Xu, *Electrochim. Acta*, 2019, **328**, 135137.
48 X. Liu, G. B. Xu, S. J. Huang, L. Li, Y. Wang and L. W. Yang, *Electrochim. Acta*, 2021, **368**, 137600.
49 N. S. W. Gamage, Y. L. Shi, C. J. Mudugamuwa, J. Santos-Peña, D. A. Lewis, J. M. Chalker and Z. F. Jia, *Energy Storage Mater.*, 2024, **72**, 103731.
50 L. P. Li, S. L. Liu, W. C. Liu, D. L. Ba, W. Y. Liu, Q. Y. Gui, Y. Chen, Z. Q. Hu, Y. Y. Li and J. P. Liu, *Nano-Micro Lett.*, 2021, **13**, 34.
51 J. Ren, P. Hong, Y. Ran, Y. H. Chen, X. C. Xiao and Y. D. Wang, *Inorg. Chem. Front.*, 2022, **9**, 792.
52 N. Wang, C. L. Sun, X. B. Liao, Y. F. Yuan, H. W. Cheng, Q. C. Sun, B. L. Wang, X. L. Pan, K. N. Zhao, Q. Xu, X. G. Lu and J. Lu, *Adv. Energy Mater.*, 2020, **10**, 2002293.
53 H. M. Jiang, Y. F. Zhang, M. Waqar, J. Yang, Y. Y. Liu, J. J. Sun, Z. Y. Feng, J. G. Sun, Z. H. Pan, C. G. Meng and J. H. Wang, *Adv. Funct. Mater.*, 2023, **33**, 2213127.
54 W. Y. Zhang, S. Q. Liang, G. Z. Fang, Y. Q. Yang and J. Zhou, *Nano-Micro Lett.*, 2019, **11**, 69.
55 H. Ma, X. C. Tian, T. Wang, K. Tang, Z. X. Liu, S. E. Hou, H. Y. Jin and G. Z. Cao, *Small*, 2021, **17**, 2100746.
56 Y. Y. Li, T. Li, Y. Shen, S. H. Yang, K. Li and T. Q. Lin, *Front. Energy*, 2025, **19**, 999–1006.
57 T. P. Jiao, Q. Yang, S. L. Wu, Z. F. Wang, D. Chen, D. Shen, B. Liu, J. Y. Cheng, H. F. Li, L. T. Ma, C. Y. Zhi and W. J. Zhang, *J. Mater. Chem. A*, 2019, **7**, 16330–16338.
58 T. Li, X. J. Dong, H. G. Yang, J. W. Zhang, R. Huang, Z. R. Lv, Y. Y. Li, S. C. Zhang, F. Q. Huang and T. Q. Lin, *Energ Environ. Sci.*, 2025, **18**, 3169–3176.
59 F. N. Mo, M. W. Cui, L. L. Yang, H. Lei, S. Chen, J. Wei and L. T. Kang, *Batteries*, 2022, **8**, 239.
60 S. A. Liu, Y. Y. Sun, J. Yang, Y. Zhang and Z. Y. Cai, *Materials*, 2022, **15**, 5954.
61 Y. Zhao, Y. X. Huang, F. Wu, R. J. Chen and L. Li, *Adv. Mater.*, 2021, **33**, 2106469.
62 L. Xu, N. Xu, C. Y. Yan, W. He, X. Y. Wu, G. W. Diao and M. Chen, *J. Electroanal. Chem.*, 2021, **888**, 115196.
63 N. Liu, B. Li, Z. X. He, L. Dai, H. Y. Wang and L. Wang, *J. Energy Chem.*, 2021, **59**, 134–159.
64 W. H. Zhang, X. L. Zhai, Y. S. Zhang, H. J. Wei, J. Q. Ma, J. Wang, L. L. Liang, Y. Liu, G. X. Wang, F. Z. Ren and S. Z. Wei, *Front. Energy Res.*, 2020, **8**, 195.
65 B. M. Zhang, J. H. Chen, W. Y. Sun, Y. B. Shao, L. Zhang and K. N. Zhao, *Energies*, 2022, **15**, 4698.
66 Y. L. Zhao, Y. H. Zhu and X. B. Zhang, *Infomat*, 2020, **2**, 237–260.
67 Y. Liu and X. Wu, *Chinese Chem. Lett.*, 2022, **33**, 1236–1244.
68 Y. H. Qian and L. Y. Chen, *J. Energy Chem.*, 2024, **99**, 553–579.

69 J. C. Wu, Y. Y. Yin, H. T. Zhou, X. C. Shen, H. Q. Gao, X. W. Li, Z. Y. Liu, Y. H. Deng and Y. X. Qiao, *Metals*, 2025, **15**, 526.
70 T. Song, W. F. Fan, Y. Hu, H. Zhang and Y. C. Bai, *Green Chem.*, 2025, **27**, 10071–10093.
71 F. R. Chen, Y. Zhang, S. Chen, H. Zang, C. J. Liu, H. X. Sun and B. Y. Geng, *J Colloid Interf. Sci.*, 2023, **649**, 703–712.
72 S. Z. Deng, Z. W. Tie, F. Yue, H. M. Cao, M. J. Yao and Z. Q. Niu, *Angew. Chem. Int. Edit*, 2022, **61**, e202115877.
73 Y. Liu and X. Wu, *J. Energy Chem.*, 2021, **56**, 223–237.
74 H. Y. Shi, H. L. Fu, G. J. Xue, Y. Lian, J. Zhao and H. H. Zhang, *Coordin. Chem. Rev.*, 2025, **545**, 216984.
75 Y. H. Wu, J. Q. Lv, X. R. Hao, Z. Q. Zhao, Y. H. Ling, L. Li, Y. Y. Guan, F. N. Shi, P. F. Wang, Y. H. Zhang, C. L. Zhang, Z. J. Wang and J. Y. Liang, *Nano Res.*, 2025, **18**, 94907573.
76 W. W. Zhang, C. L. Zuo, C. Tang, W. Tang, B. X. Lan, X. D. Fu, S. J. Dong and P. Luo, *Energy Technol-Ger.*, 2021, **9**, 2000789.
77 Y. Wu, Q. Zhao and Z. Wang, *Chin. J. Struct. Chem.*, 2024, **43**, 100271.
78 T. H. Wu, T. K. Li and L. J. Guo, *J. Power Sources*, 2024, **623**, 235503.
79 J. X. Wu, F. Ciucci and J. K. Kim, *Chem.–Eur. J.*, 2020, **26**, 6296–6319.
80 L. F. Wang, Z. Xu, W. L. Wang and X. D. Bai, *J. Am. Chem. Soc.*, 2014, **136**, 6693–6697.
81 Y. C. Jiao, A. M. Hafez, D. X. Cao, A. Mukhopadhyay, Y. Ma and H. L. Zhu, *Small*, 2018, **14**, 1800640.
82 D. X. Wu, C. Y. Wang, M. G. Wu, Y. F. Chao, P. B. He and J. M. Ma, *J. Energy Chem.*, 2020, **43**, 24–32.
83 T. Li, H. X. Li, J. C. Yuan, Y. Xia, Y. J. Liu and A. K. Sun, *Materials*, 2022, **15**, 2654.
84 M. H. Wu, C. Shi, J. W. Yang, Y. Zong, Y. Chen, Z. G. Ren, Y. X. Zhao, Z. Li, W. Zhang, L. Y. Wang, X. L. Huang, W. Wen, X. L. Li, X. Ning, X. C. Ren and D. M. Zhu, *Adv. Mater.*, 2024, **36**, 2310434.
85 A. Y. Su, Q. Pang, X. Chen, J. J. Dong, Y. Y. Zhao, R. Q. Lian, D. Zhang, B. B. Liu, G. Chen and Y. J. Wei, *J. Mater. Chem. A*, 2018, **6**, 23357–23365.
86 M. X. Tran, G. C. Liu, S. W. Lee and J. K. Lee, *Appl. Surf. Sci.*, 2024, **669**, 160523.
87 S. S. Yao, H. L. Yu, M. Z. Bi, C. J. Zhang, T. J. Zhang, X. N. Zhang, H. T. Liu, X. Q. Shen and J. Xiang, *Int. J Energ. Res.*, 2022, **46**, 19585–19598.
88 Y. Hwa and E. J. Cairns, *Electrochim. Acta*, 2018, **271**, 103–109.
89 X. Y. Zhou, X. Z. Peng, X. Y. Feng, X. W. Gao, M. K. Li, H. F. Ji, G. D. Liu, Y. Feng and X. J. Zhang, *Acs Appl. Energ. Mater.*, 2025, **8**, 7644–7654.
90 H. Liu, J. Sun, P. Y. Sun, C. Y. Zhao, T. Ma, X. J. Shi, Y. Z. Wang and Y. J. Wei, *Small*, 2025, **21**, 2503069.
91 Y. H. Li, X. Y. Ren, D. W. Zhang, S. H. Ju, W. Hu, T. Hang, M. Li and Y. W. Wu, *Adv. Funct. Mater.*, 2025, e14665.
92 W. J. Zheng, Z. B. Cui, C. Liu, L. B. Yuan, S. S. Li, L. L. Lin, T. Meng, L. G. Yang, Y. X. Tong and D. Shu, *Chem. Sci.*, 2024, **15**, 20303–20314.
93 L. P. Zhang, Y. Y. Li, X. J. Liu, R. P. Yang, J. X. Qiu, J. K. Xu, B. Y. Lu, J. Rosen, L. Q. Qin and J. X. Jiang, *Adv. Sci.*, 2024, **11**, 2401252.
94 X. Zhang, Y. C. Tang, P. G. He, Z. Zhang and T. F. Chen, *Carbon*, 2021, **172**, 207–213.
95 J. W. Long, T. L. Han, X. R. Lin, Y. J. Zhu, Y. Y. Ding, J. Y. Liu and H. G. Zhang, *Nano Res.*, 2023, **16**, 11000–11011.
96 J. Y. Zhang, R. A. Liu, C. Huang, C. Q. Dong, L. Xu, L. Y. Yuan, S. G. Lu, L. L. Wang, L. Zhang and L. Y. Chen, *Nano Energy*, 2024, **122**, 109301.
97 Y. M. Zhang, S. Y. Jiang, Y. L. Li, X. Z. Ren, P. X. Zhang, L. N. Sun and H. Y. Yang, *Adv. Energy Mater.*, 2023, **13**, 2202826.
98 X. M. Liu, D. Zhao and J. H. Wang, *Nano-Micro Lett.*, 2024, **16**, 157.
99 Q. D. Bao, X. T. Zhang, Z. K. Hao, Q. H. Li, F. Wu, K. Y. Wang, Y. Li, W. L. Li and H. Gao, *Nano-Micro Lett.*, 2024, **16**, 268.
100 D. F. Ji, H. Y. Zheng, H. Zhang, W. Q. Liu and J. W. Ding, *J. Alloys Compd.*, 2022, **900**, 163394.
101 D. F. Ji, H. Y. Zheng, H. Zhang, W. Q. Liu and J. W. Ding, *Chem. Eng. J.*, 2022, **433**, 133815.
102 Y. T. Liu, H. K. Ding, H. L. Chen, H. X. Gao, J. X. Yu, F. N. Mo and N. Wang, *Polymers*, 2025, **17**, 2136.
103 L. Wu and Z. C. Dong, *Adv. Mater.*, 2023, **35**, 2300903.

